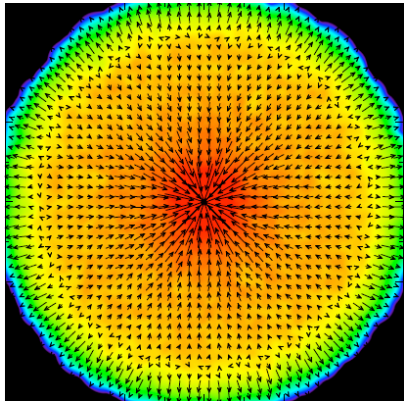
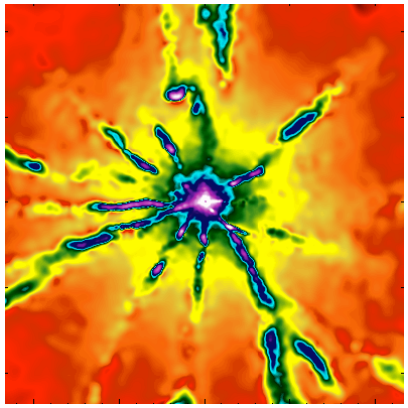
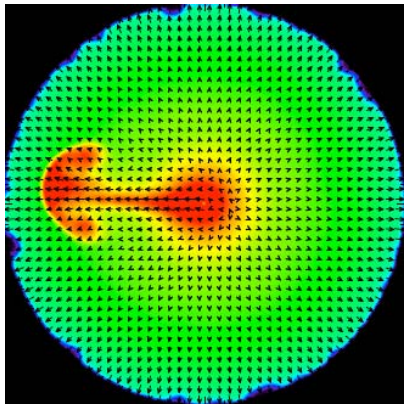

Simulating Supermassive Black Hole Accretion: Spherical Flow to Cold Clumps & Hot Bubbles

Paramita Barai

UNLV
UNIVERSITY OF NEVADA LAS VEGAS

Collaborators: Daniel Proga, Kentaro Nagamine

Gas Dynamics and Star Formation in the Extreme Environment of Galactic Nuclei - Ringberg, Germany

21 March, 2013

Small-scale sim (Proga & Begelman 2003, Proga Ostriker & Kurosawa 2008)

Cosmological sim (Di Matteo, Springel & Hernquist 2005, Booth & Schaye 2009)

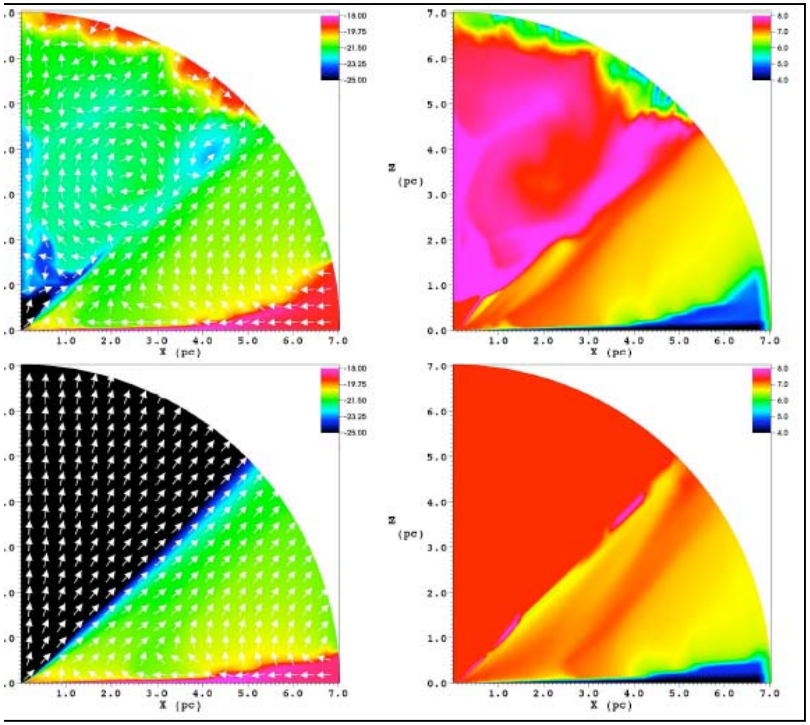

Motivation

Large dynamic range of length scales

$\longleftrightarrow$

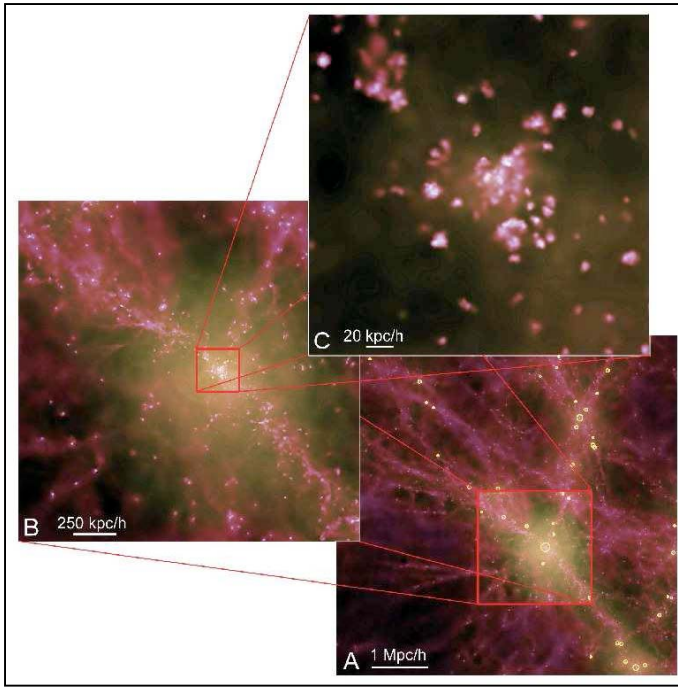

BH accretion:

Galaxy physics:

$$M_{\rm BH} = 10^8 M_{\rm sun} : R_{\rm Sch} \sim 10^{-5}\,{\rm pc} \Rightarrow R_{\rm sonic} \sim 1-10{\rm s}\ {\rm pc} \Rightarrow R_{\rm gal} \sim 10^3 - 10^6 {\rm pc}$$

- Challenging: Cosmological simulations cannot resolve the Sonic Point, which is important to properly model BH accretion
- Previous subgrid models of AGN feedback in galaxy formation have assumed the Bondi-Hoyle accretion rate, with ad-hoc choice of parameter values

Outline

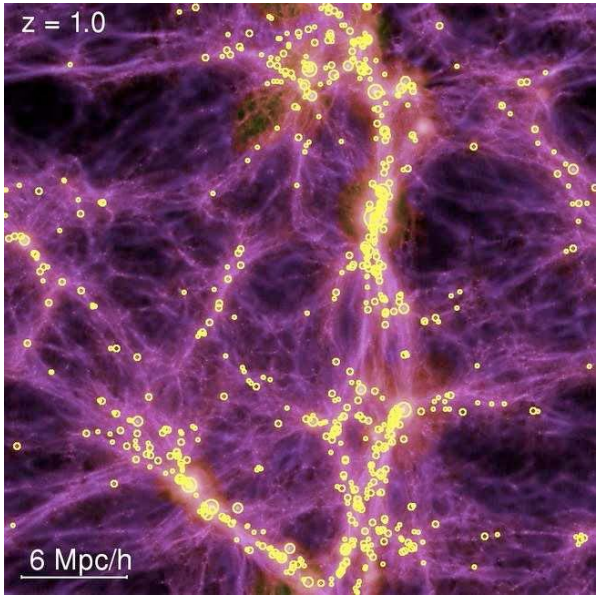

- Use cosmological / galaxy formation code to simulate BH accretion on smaller scales

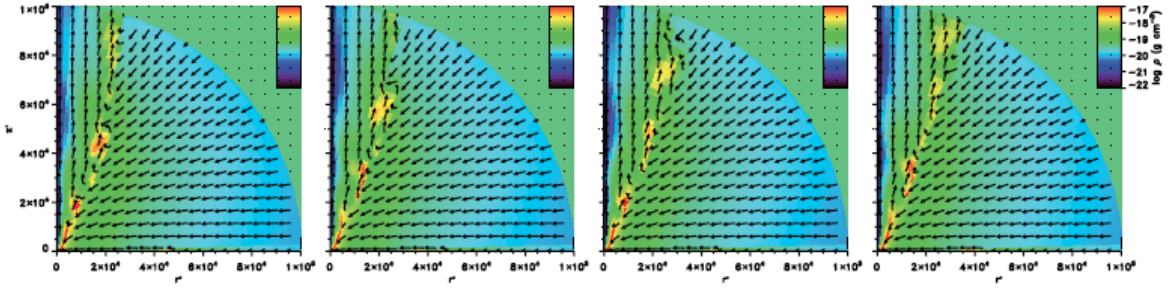

- Smoothed-Particle Hydrodynamics (SPH)
  - Can handle large dynamical range
- Use 3D Tree-PM SPH code GADGET-III
  - (Springel, V. 2005, MNRAS, 364, 1105)
- First Test : How well can SPH simulate Bondi accretion onto a SMBH?
- Radiative heating & cooling, feedback
- Instability driven clumps & bubbles

Barai, Proga & Nagamine (2011, 2012)

Reproduce Original Bondi Problem

- Spherically-symmetric accretion of gas having given density ρ and temperature ($T \rightarrow c_s$) at infinity
  (Bondi 1952, MNRAS, 112, 195)

- Mass accretion rate :

$$\dot{M}_{acc} = \lambda(4\pi)\frac{(GM_{BH})^2 \rho_\infty}{c_{s,\infty}^3}$$

$$= \frac{1}{4} \text{ , for, } \# = \frac{5}{3}$$

- Bondi radius and time :

$$R_{Bondi} = \frac{GM_{BH}}{c_{s,\infty}^2}, \quad t_{Bondi} = \frac{R_{Bondi}}{c_{s,\infty}}$$

- Sonic point:

$$R_{sonic} = \text{fn}(\gamma) \times R_{Bondi}$$

Simulation Setup

- Spherical distribution of gas accreting onto a SMBH
- Central BH represented with a static Paczynsky-Wiita potential
  (Paczynsky & Wiita 1980, A&A, 88, 23)

$$M_{BH} = 10^8 M_{Sun}$$

$$\Psi_{PW} = \frac{GM_{BH}}{\left(r - R_{Sch}\right)}$$

- r_{in} = 0.1 pc, r_{out} = 5, 10, 20, 200 pc
  - Must encompass R_{Bondi} & R_{sonic} inside
- BH Sink inside r_{in}
  ⇒ Gas accreted in, & removed from sim.

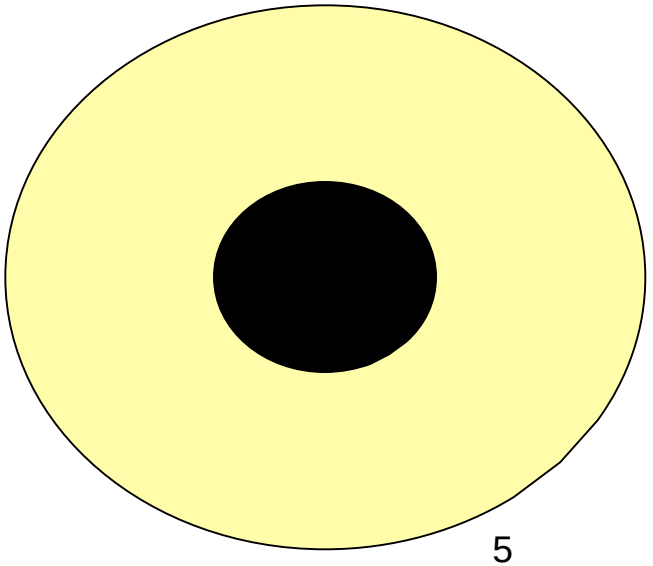

Simulations of Bondi Accretion

Run No.	r_{out} [pc]	N [b]	IC	$M_{tot,IC}$ [c] $[M_\odot]$	M_{part} [d] $[M_\odot]$	t_{end} [e] $[10^4$ yr]
1	5	64^3	Uniform [i]	3.96×10^5	1.51	3
2	10	64^3	Uniform	6.19×10^6	23.61	7.2
3	50	128^3	Uniform	7.73×10^8	368.60	20
4	5	64^3	Bondi [j]	1.81×10^6	6.89	2
5	10	64^3	Bondi	9.76×10^6	37.23	8
6	10	128^3	Bondi	9.76×10^6	4.65	8
7	20	128^3	Bondi	6.24×10^7	29.75	8
7a [k]	20	128^3	Bondi	6.24×10^7	29.75	80
7b [l]	20	128^3	Bondi	6.24×10^7	29.75	100
8	50	128^3	Bondi	8.48×10^8	404.35	16
9	20	128^3	$\rho_B, v_{init} = 0$	6.24×10^7	29.75	8
10	20	128^3	Uniform	4.95×10^7	23.60	8
11	20	128^3	Hernquist [m]	6.24×10^7	29.75	7.2
12 [n]	20	128^3	Bondi	6.24×10^7	29.75	8

- All runs have

$r_{in} = 0.1$ pc

$\gamma = 1.01$

$\rho_\infty = 10^{-19}$ g/cm^3

$T_\infty = 10^7$ K

Gas Properties

- Black: Gas particles from sim Run 7 at time = 2 t_{Bondi} = 1.6 x 10^4 yr
- Red: Bondi solution
  - Well reproduced
- Gas inflow from sub- to super-sonic reaching Mach ~ 6
- Issues:
  - Discrepancy near r_{in} → AV
  - Outer boundary: Outflow at r_{out}, because of finite pressure gradient

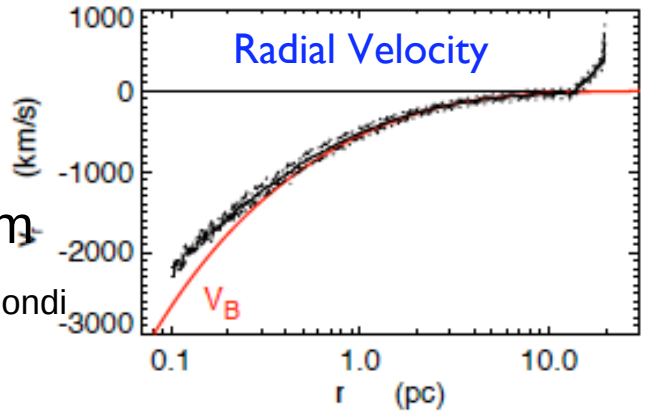

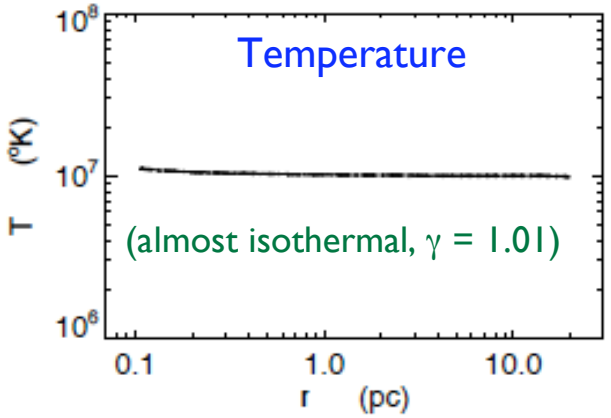

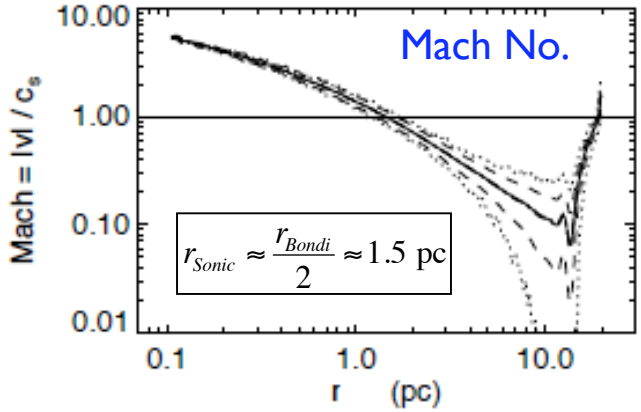

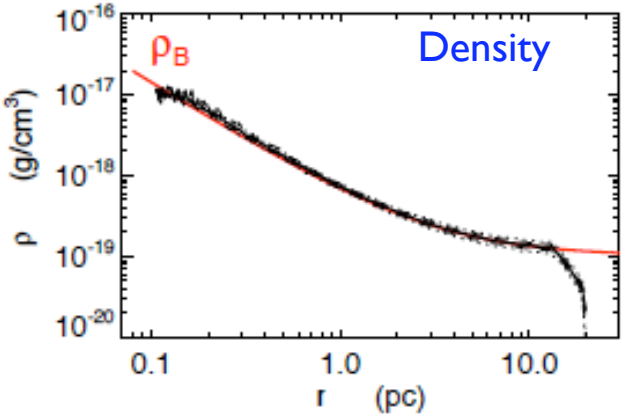

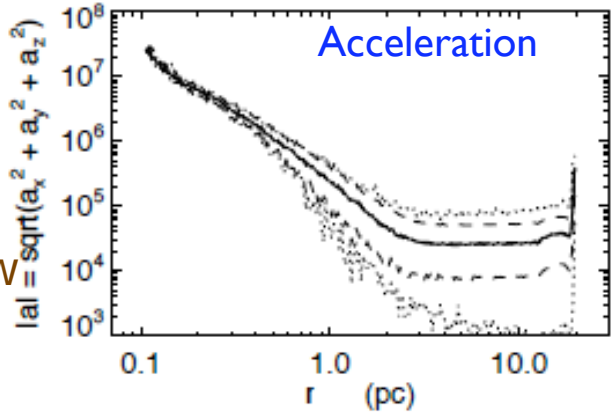

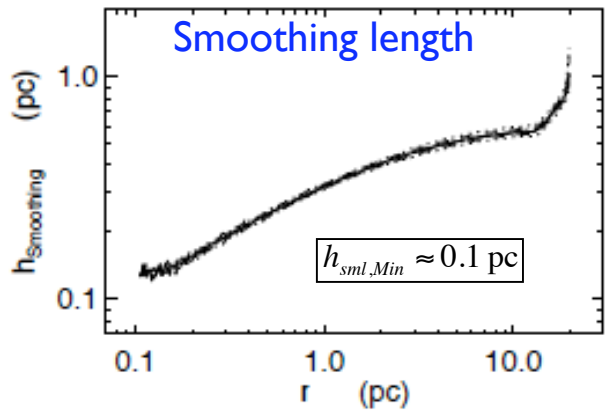

Mass Inflow Rate at r_{in}

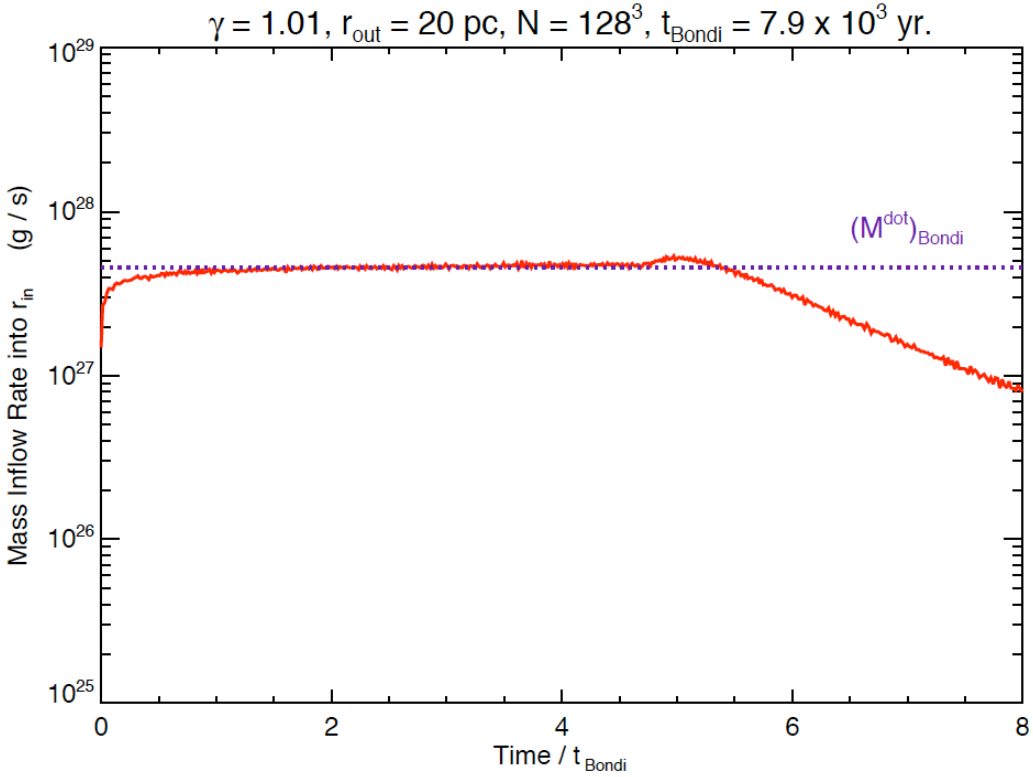

- Bondi solution is reproduced within $4t_{Bondi}$ (for 4×10^4 yrs)

- Spherically-Symmetric Gas Properties

- Duration of Bondi inflow rate increases with r_{out}
- Bondi accretion rate is reached starting with different IC density profiles
  - Bondi
  - Uniform
  - Hernquist

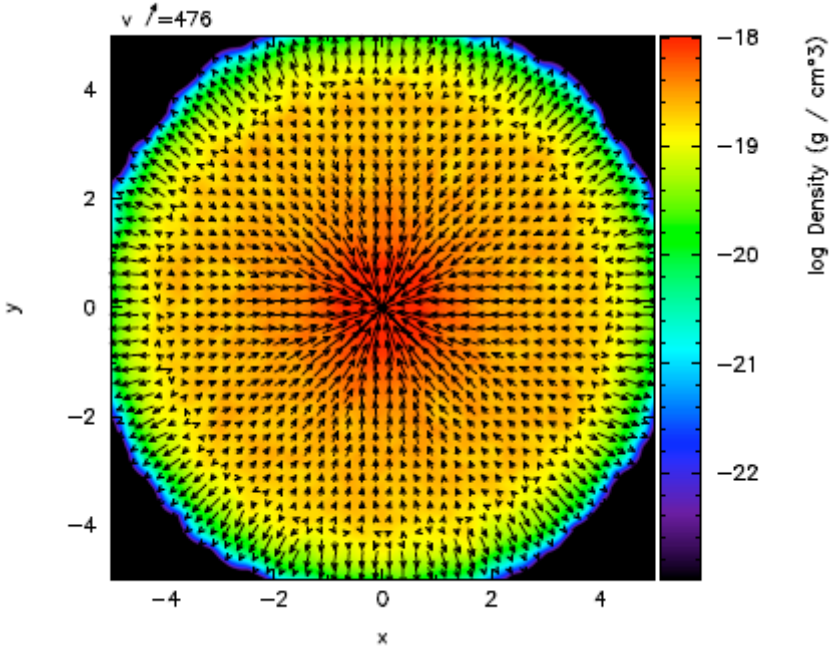

Add Radiative Heating & Cooling

- Spherical X-ray corona of luminosity L_X around central BH
  (Kurosawa & Proga 2009, MNRAS, 397, 1791)

$$L_X = f_X L_{Edd}, \qquad L_{Edd} = \frac{4\pi c G m_p M_{BH}}{\sigma_e}$$

- Photoionization parameter :

$$\xi \equiv \frac{4\pi F_X}{n} = \frac{L_X}{r^2 n}$$

- Assume : optically thin gas

- Net Heating-Cooling rate
  (Blondin 1994, ApJ, 435, 756)
  (Proga, Stone & Kallman, T.R. 2000, ApJ, 543, 686)

$$\rho\mathcal{L} = n^2 \left(G_{\rm Compton} + G_X - L_{b,l}\right) \quad [\rm erg\ cm^{-3}\ s^{-1}],$$

- Added to eqn of hydrodynamics

$$\rho \frac{D}{Dt}\left(\frac{e}{\rho}\right) = -P\nabla \cdot \boldsymbol{v} + \rho\mathscr{L},$$

Components

- Approximate analytic formulae for X-ray irradiated optically-thin gas, in the presence of 10 keV Bremsstrahlung spectrum (Blondin 1994)
  - $T_X = 1.16 \times 10^8$ K

- Compton heating-cooling

$$G_{\rm Compton} = 8.9 \times 10^{-36} \xi \left(T_X - 4T\right) \quad [{\rm erg\,cm^3\,s^{-1}}].$$

- X-ray photoionization heating - recombination cooling

$$G_X = 1.5 \times 10^{-21} \xi^{1/4} T^{-1/2} \left(1 - \frac{T}{T_X}\right) \quad [{\rm erg\ cm^3\ s^{-1}}].$$

- Bremsstrahlung & metal line cooling

$$\begin{aligned} L_{b,l} \quad = \quad & 3.3 \times 10^{-27} T^{1/2} \\ & + \left[1.7 \times 10^{-18} \exp\left(-1.3 \times 10^5 / T\right) \xi^{-1} T^{-1/2} \right. \\ & \left. + 10^{-24}\right] \delta \qquad [{\rm erg\ cm^3\ s^{-1}}]. \end{aligned}$$

Simulations with Heating & Cooling

Run No.	r_{out} [pc]	N	$M_{tot,IC}$ [$M_\odot$]	M_{part} [$M_\odot$]	γ_{init}	T_∞ [K]	R_B [pc]	ρ_∞ [g/cm^3]	T_{init}	L_X [L_{Edd}]	t_{end} [10^5 yr]
13	20	128^3	5.81×10^5	0.277	1.4	10^7	2.19	10^{-21}	T_∞	0.5	1.0
14	50	128^3	8.23×10^6	3.92	1.4	10^7	2.19	10^{-21}	T_∞	0.5	2.9
15	20	128^3	5.81×10^{-1}	2.77×10^{-7}	1.4	10^7	2.19	10^{-27}	T_∞	0.5	1.0
16	20	256^3	5.81×10^{-1}	3.46×10^{-8}	1.4	10^7	2.19	10^{-27}	T_∞	5×10^{-4}	1.9
17	20	128^3	5.81×10^5	0.277	1.4	10^7	2.19	10^{-21}	T_{rad} [b]	5×10^{-4}	2.9
18	20	128^3	5.65×10^5	0.269	5/3	10^7	1.84	10^{-21}	T_{rad}	5×10^{-4}	3.0
19	20	128^3	1.47×10^7	7.0	5/3	10^5	183.9	10^{-21}	T_{rad}	5×10^{-4}	1.5
20	200	256^3	1.33×10^9	79.09	5/3	10^5	183.9	10^{-21}	T_{rad}	5×10^{-4}	6.5
21	200	256^3	4.95×10^8	29.50	5/3	10^7	1.84	10^{-21}	T_{rad}	5×10^{-4}	8.7
22	200	128^3	1.33×10^7	6.33	5/3	10^5	183.9	10^{-23}	T_{rad}	5×10^{-4}	70
23	200	256^3	1.33×10^7	0.791	5/3	10^5	183.9	10^{-23}	T_{rad}	5×10^{-4}	20
24 [c]	200	1.24×10^7	9.77×10^6	0.791	5/3	10^5	183.9	10^{-23}	T_{Run23}	5×10^{-5}	19
25	200	1.24×10^7	9.77×10^6	0.791	5/3	10^5	183.9	10^{-23}	T_{Run23}	5×10^{-3}	21
26	200	1.24×10^7	9.77×10^6	0.791	5/3	10^5	183.9	10^{-23}	T_{Run23}	1×10^{-2}	22
27	200	1.24×10^7	9.77×10^6	0.791	5/3	10^5	183.9	10^{-23}	T_{Run23}	2×10^{-2}	25
28	200	1.24×10^7	9.77×10^6	0.791	5/3	10^5	183.9	10^{-23}	T_{Run23}	5×10^{-2}	50

$$r_{in} = 0.1 \text{ pc}, \gamma = \frac{5}{3}$$

Gas Properties (w/ Heat-Cool)

- Black: Gas particles from sim Run 23 at time = 1 Myr
- Red: free-fall scaling w/ (adiabatic + radiative) terms
- Blue: ZEUS code (grid-based, 2D) results
- Green (T-panel, bottom-left): free-fall w/ adiabatic only
- Excess heating near r_{in} - AV
- Inner mass inflow rate > Bondi rate,
  - since $T(r_{out}) < T_{\infty} = 10^5$ K

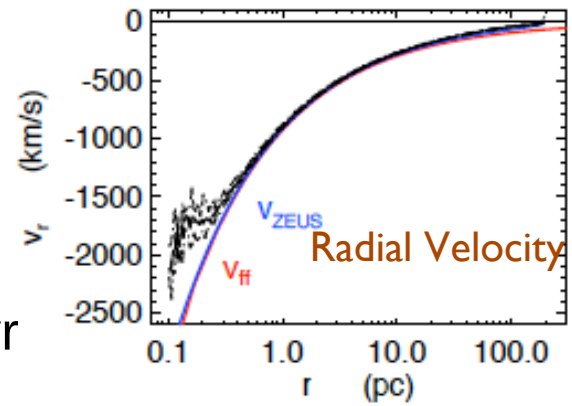

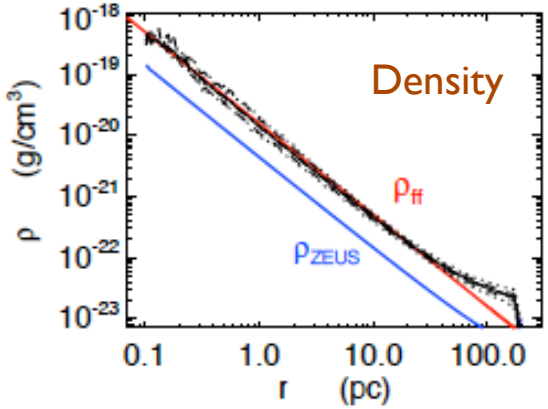

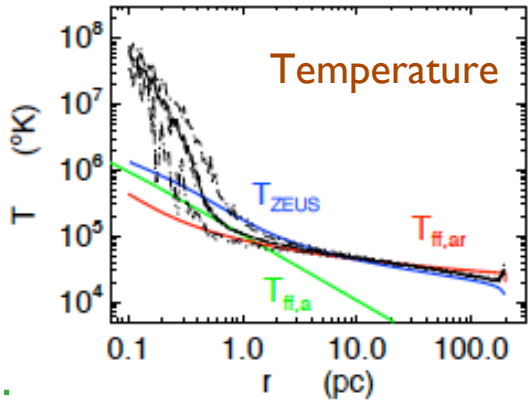

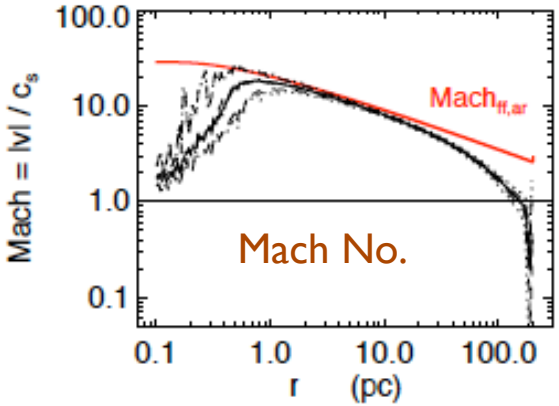

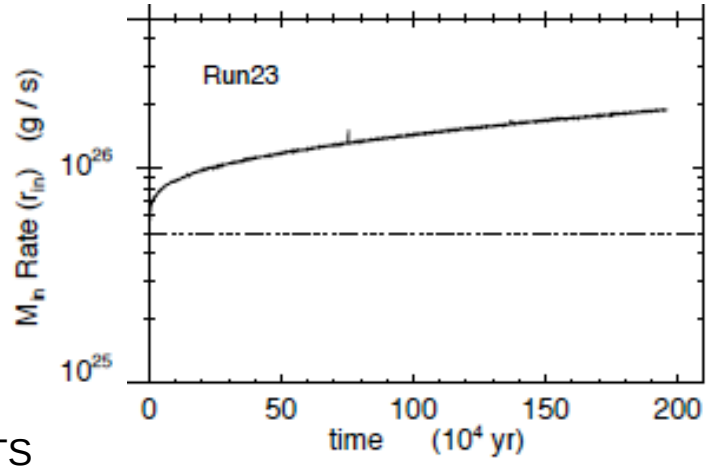

P. Barai, INAF-OATS

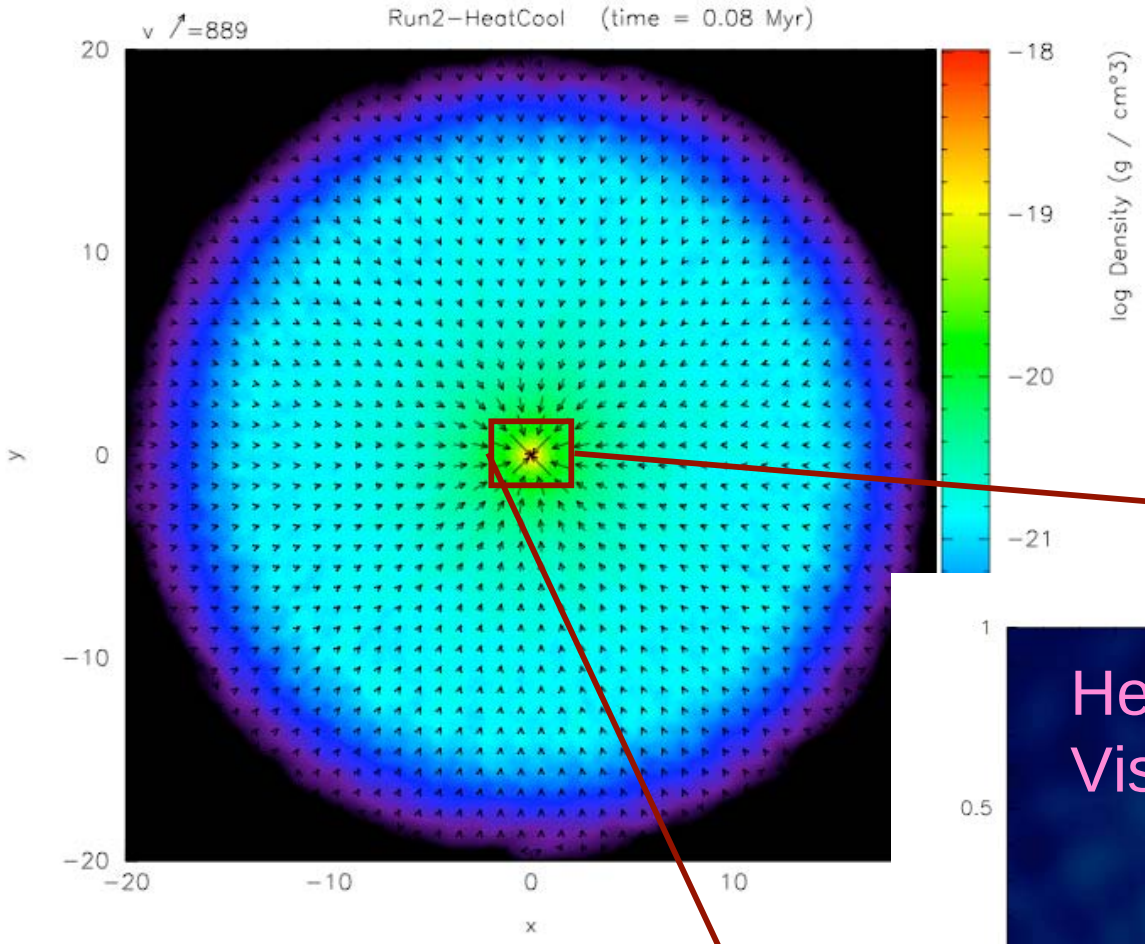

Density & velocity vectors of a cross-section slice

Run 23

Spherically-Symmetric

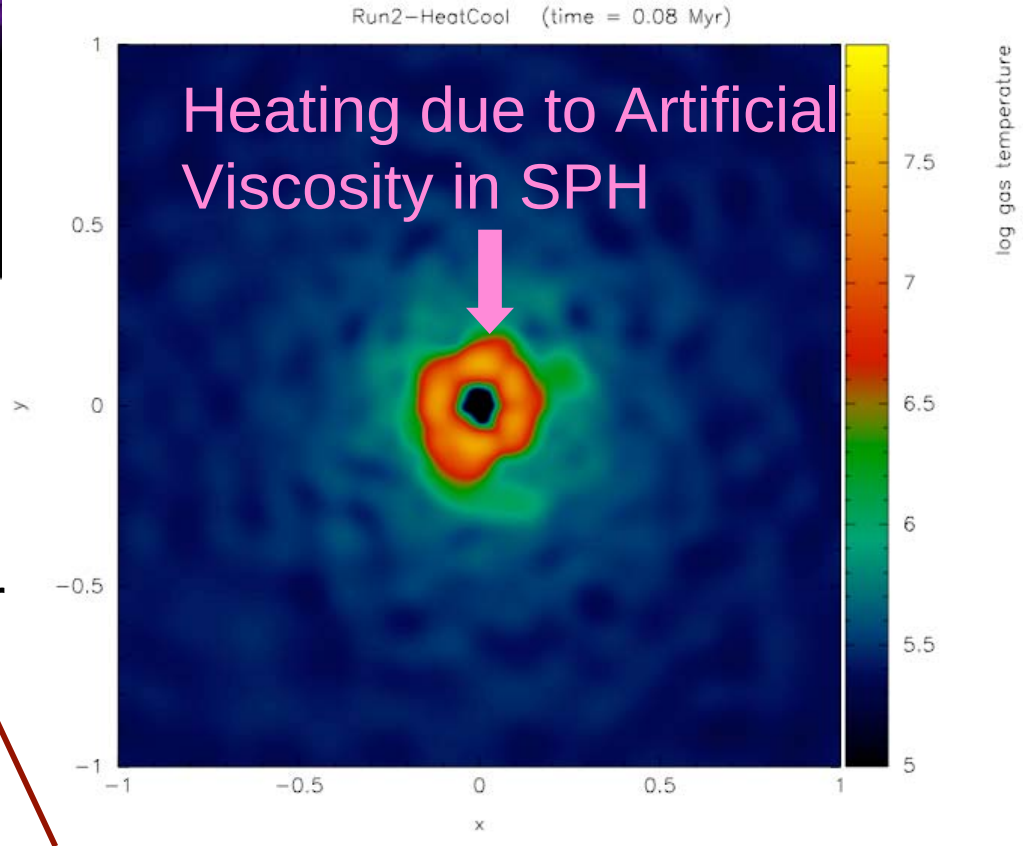

Temperature in zoomed inner region

Artificial Viscosity Heating

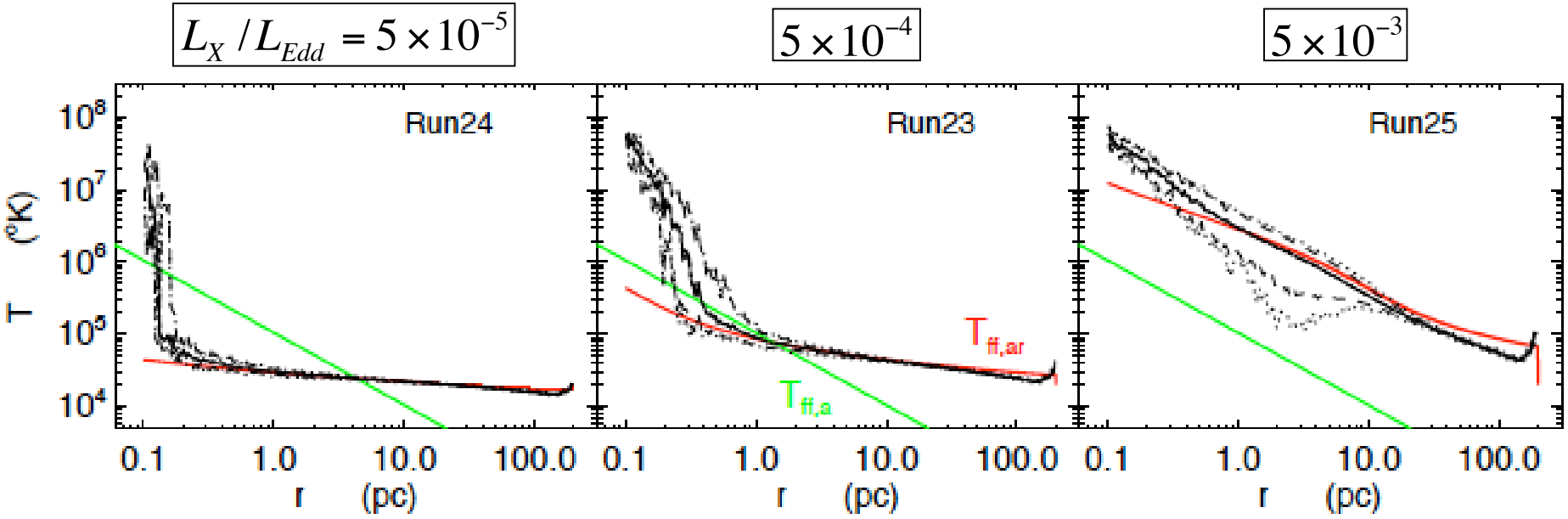

- Black: Gas particles from 3 runs at t = 1.6 Myr
- Red: free-fall scaling w/ (adiabatic + radiative) terms
- Green: free-fall w/ adiabatic term only

⇒ Shows the importance of code testing

- Alternative AV scheme (Cullen & Dehnen 2010, MNRAS, 408, 669)

Radiative Feedback

- Accreting gas undergoes feedback by radiative heating

- Increasing L_X reduces mass inflow rate, produces outflow

Change of Accretion Flow by Varying L_x

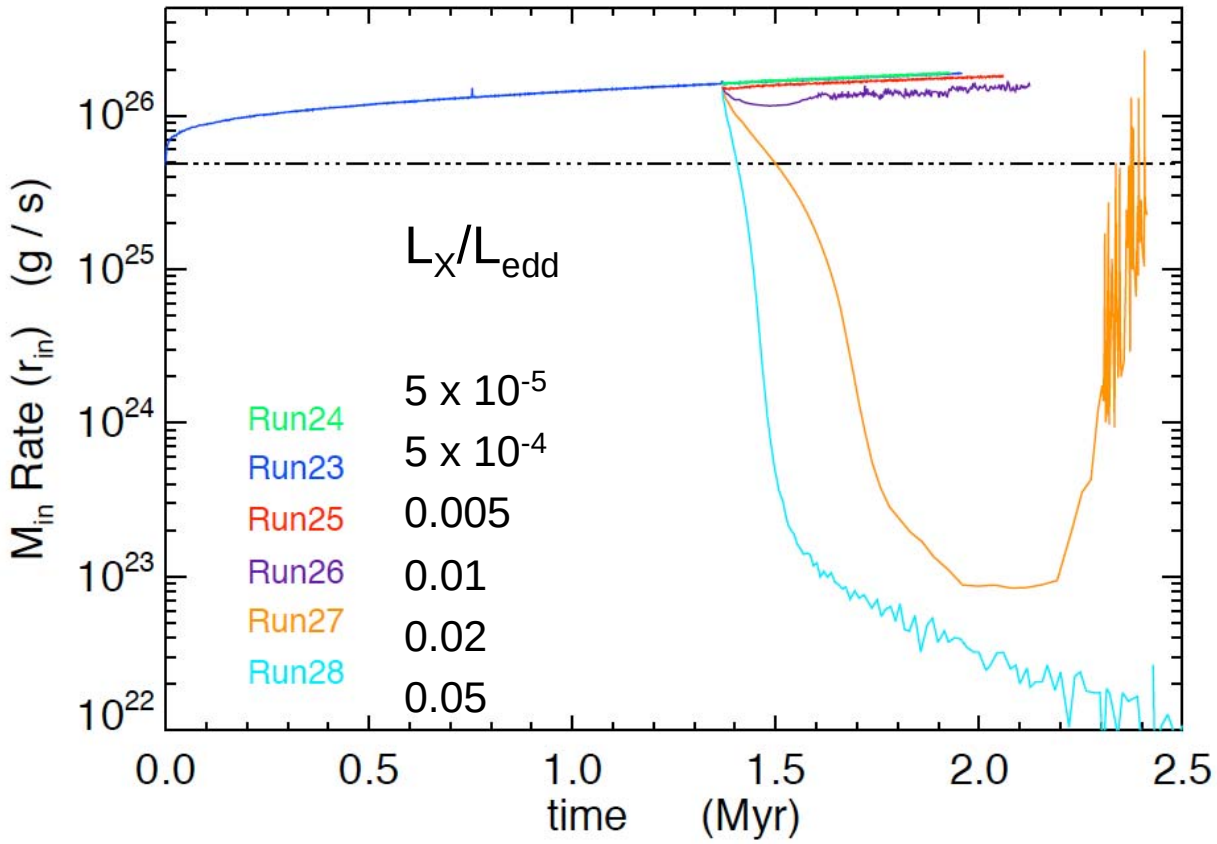

- Run 23 restarted at t = 1.4 Myr, & other runs done with varying L_x
- At $L_x \geq 0.01$, net inflow changes to net outflow
- Non-Spherical Behavior for L_x = 0.01 - 0.05 :
  - Non-uniform cooling
  - Cold regions get denser ⇒ Fragmentation & Clumping
  - Multi-phase gas motion
  - Hot Bubbles rising buoyantly from center
- Because of TI

Run 26, $L_X / L_{Edd} = 0.01$

Density

Inner 40 pc

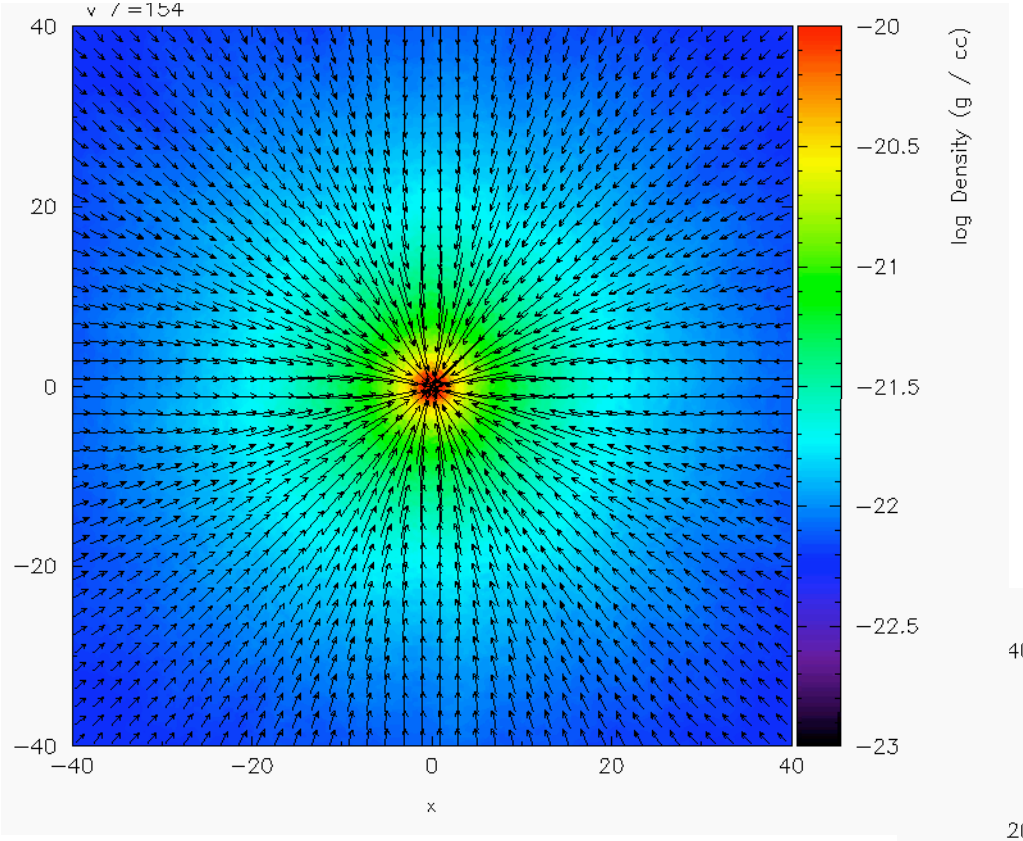

Temperature

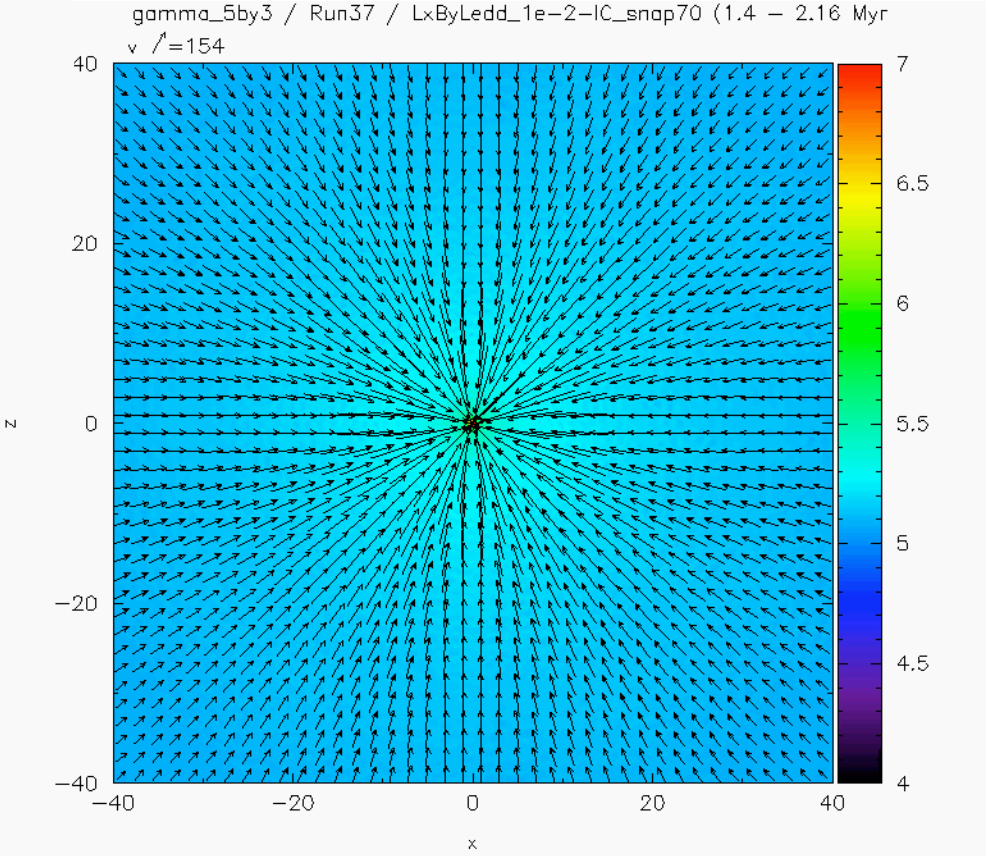

Run 26, $L_X / L_{Edd} = 0.01$

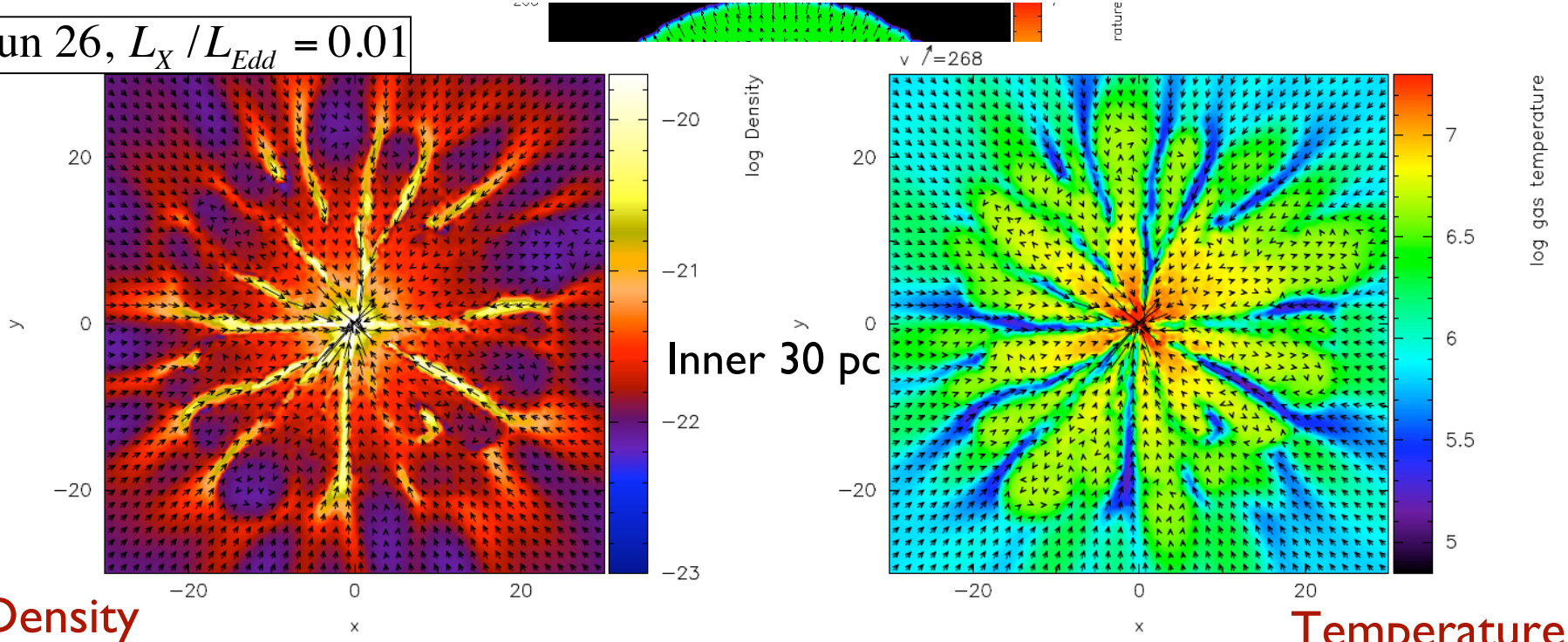

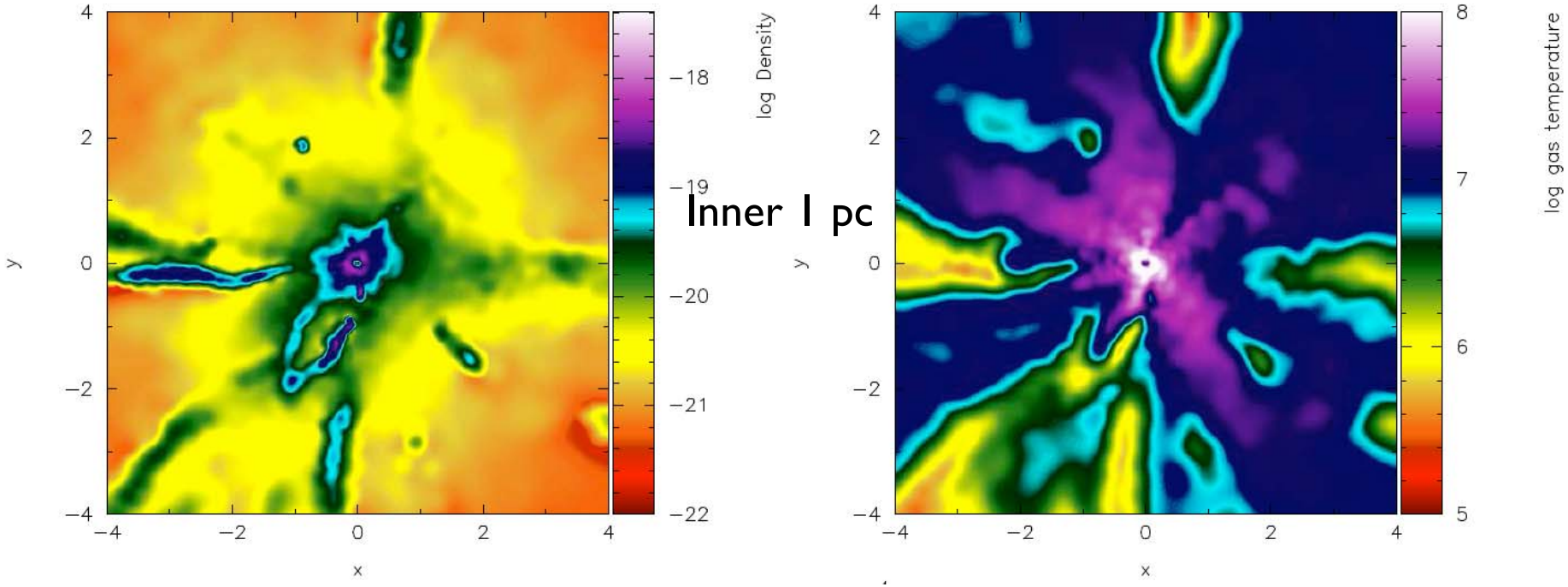

Multiphase Gas Properties

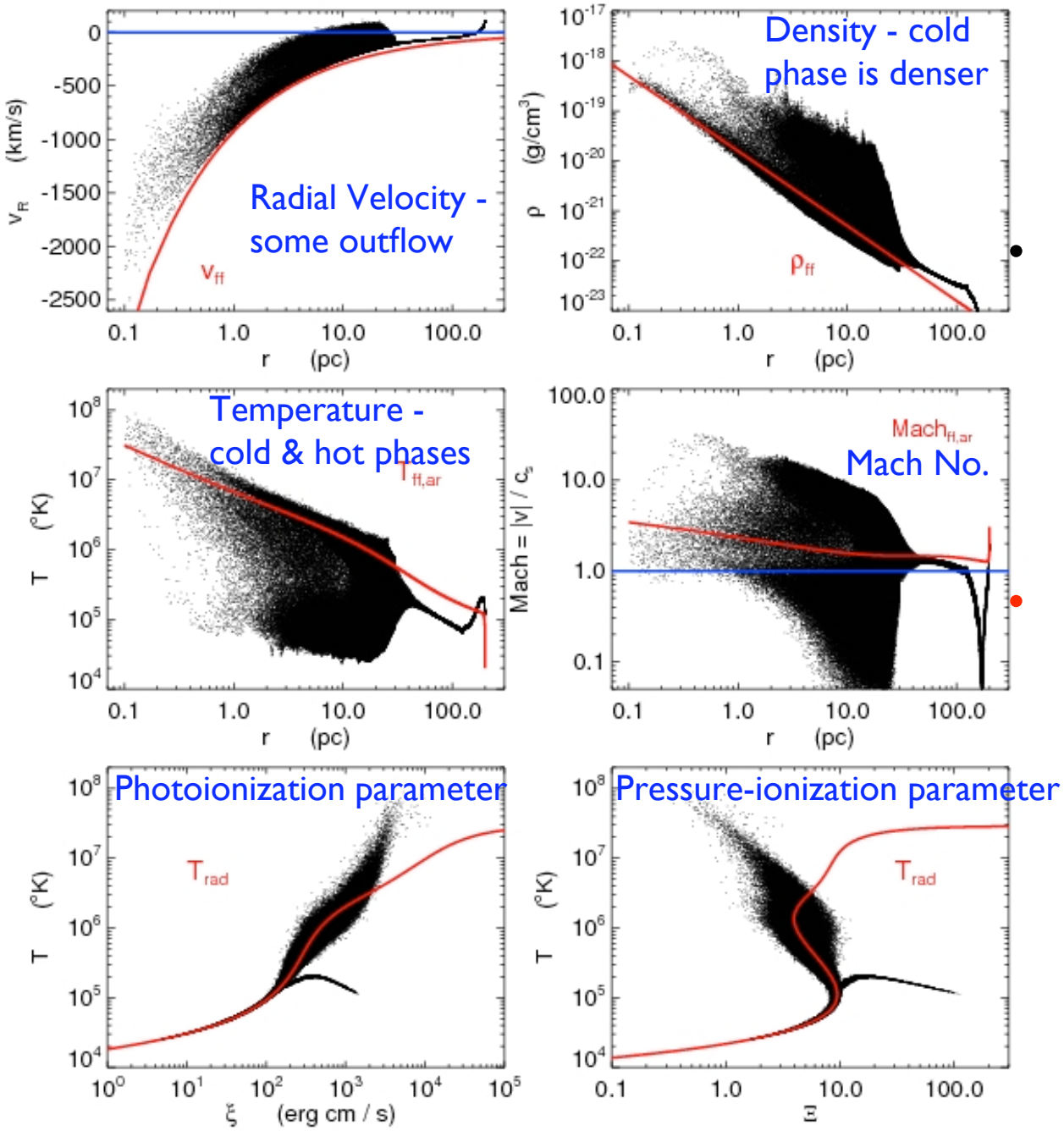

- Black: Gas particles from sim Run 26 at t = 2 Myr
  - Large scatter
  - Cooling & fragmentation caused by TI
- Red
  - Top 4 panels: free-fall scaling w/ (adiabatic + radiative) terms
  - Bottom 2: radiative equilibrium

$$\xi = \frac{L_X}{r^2 n} \qquad \Xi = \frac{F_X}{c P_{gas}}$$

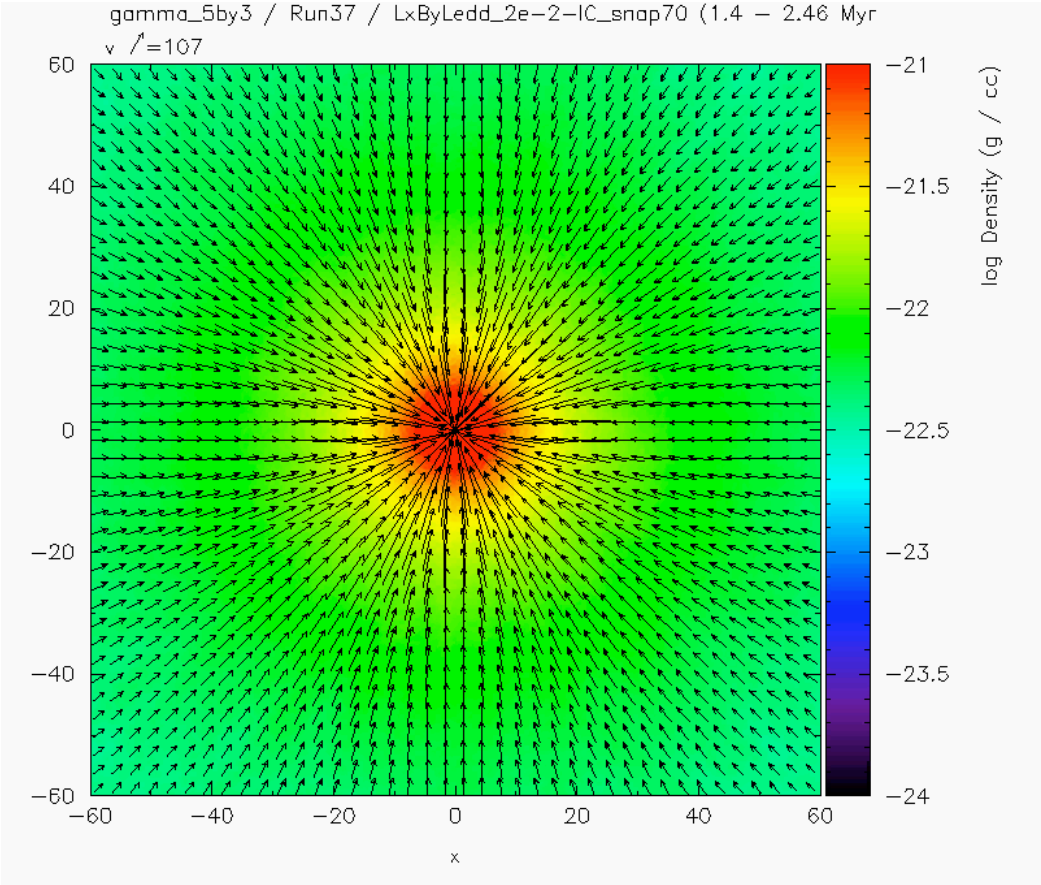

Run 27, $L_X / L_{Edd} = 0.02$

Density

Inner 60 pc

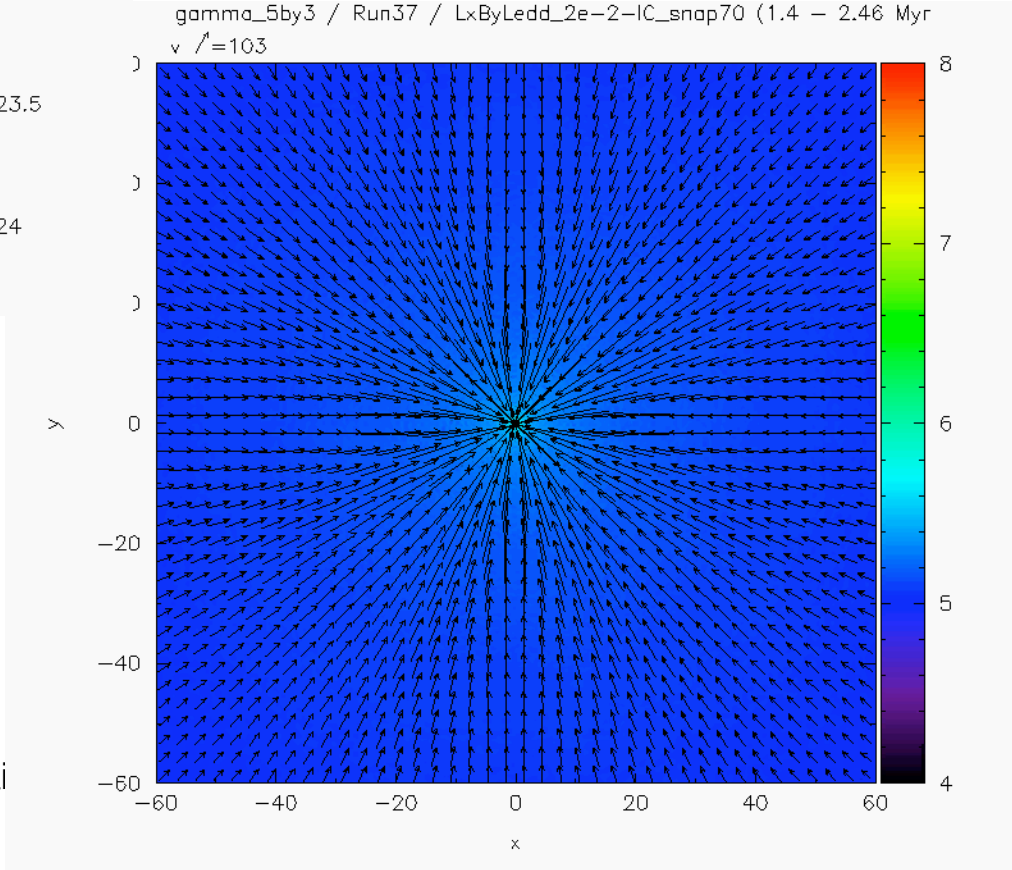

Temperature

Run 27, $L_X / L_{Edd} = 0.02$

Inner 100 pc

t = 1.86 Myr

t = 2.12 Myr

t = 2.46 Myr

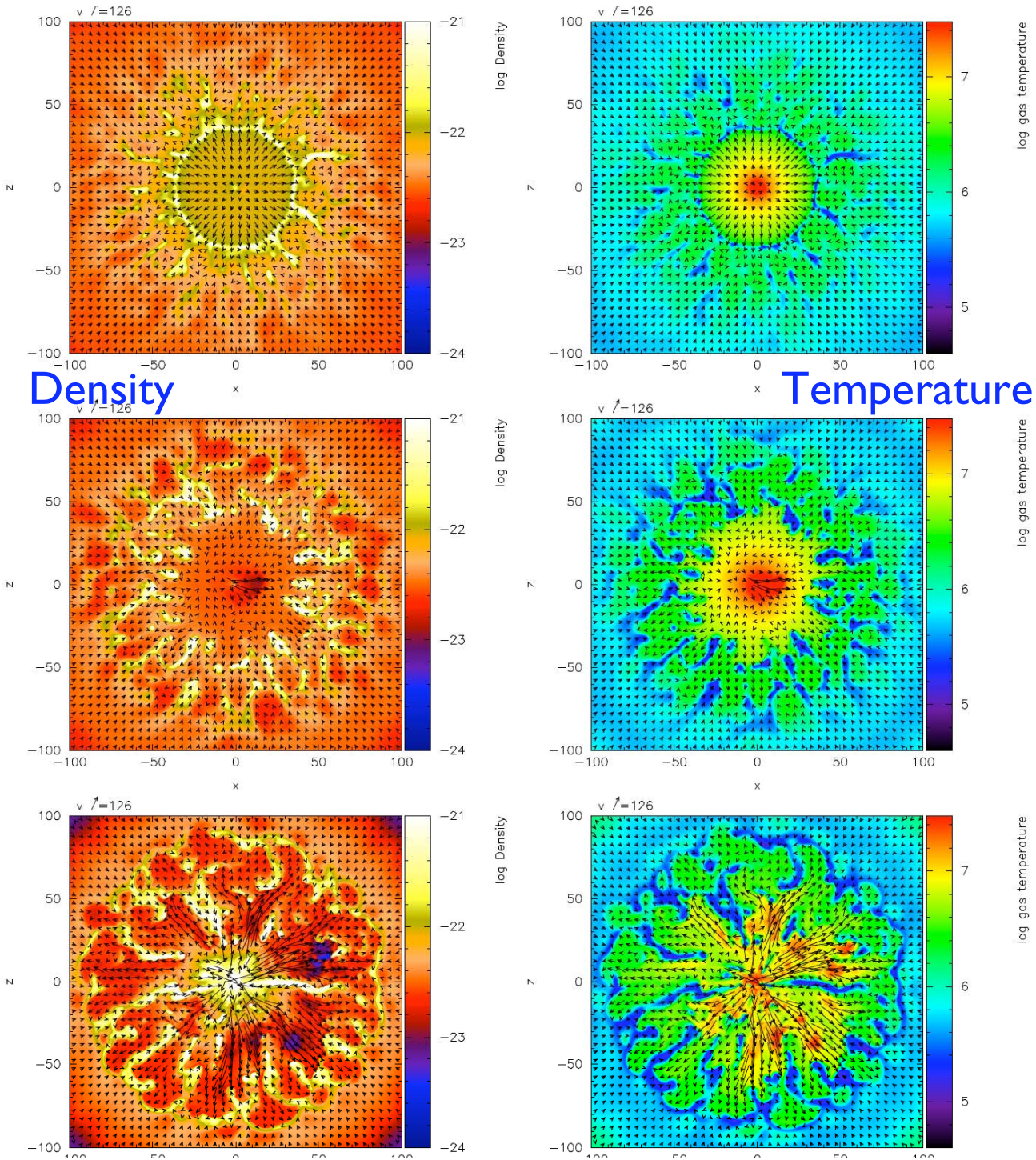

22-mars-13

$$\text{Run } 28,\ L_X / L_{Edd} = 0.05$$

Density

Whole 200 pc

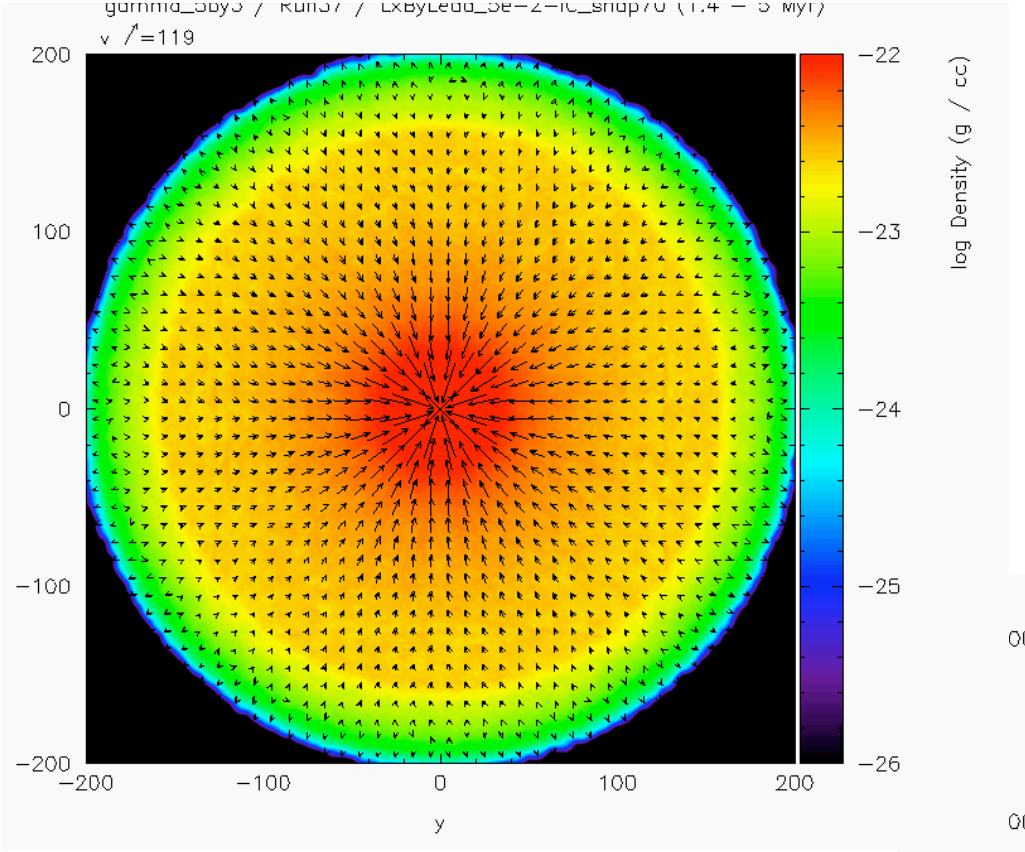

Temperature

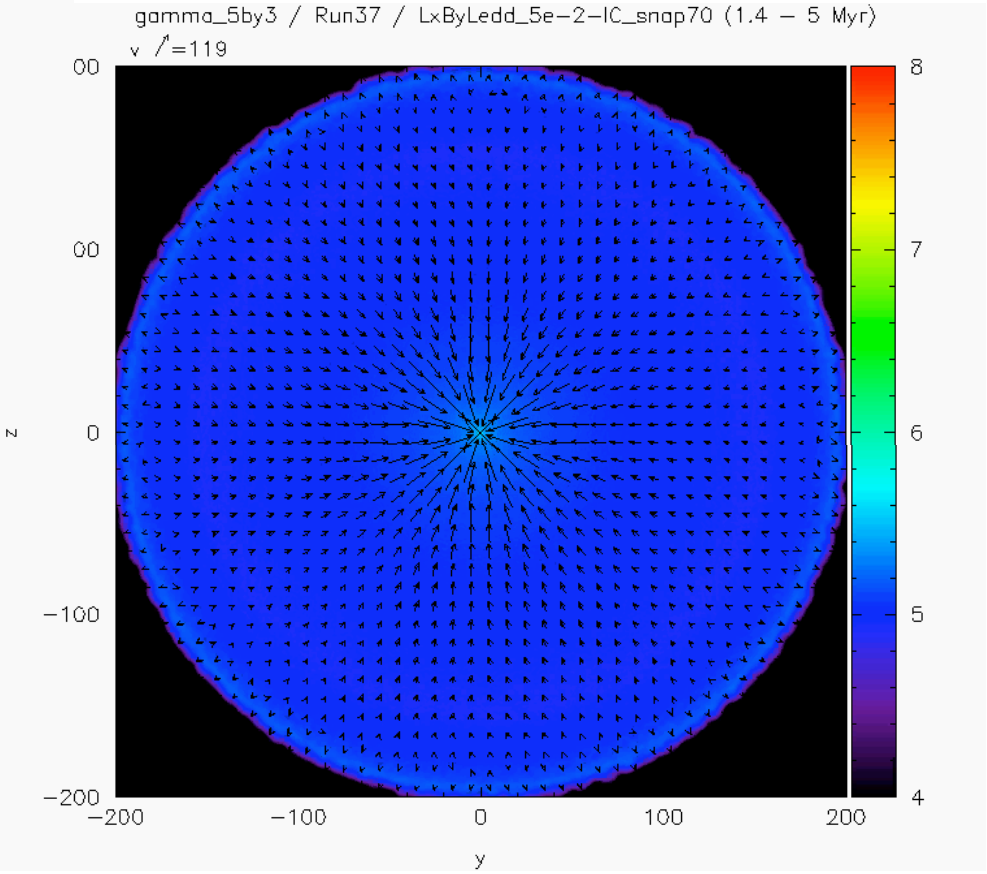

Run 28, $L_X / L_{Edd} = 0.05$

Whole 200 pc

Density

Temperature

t = 1.8 Myr

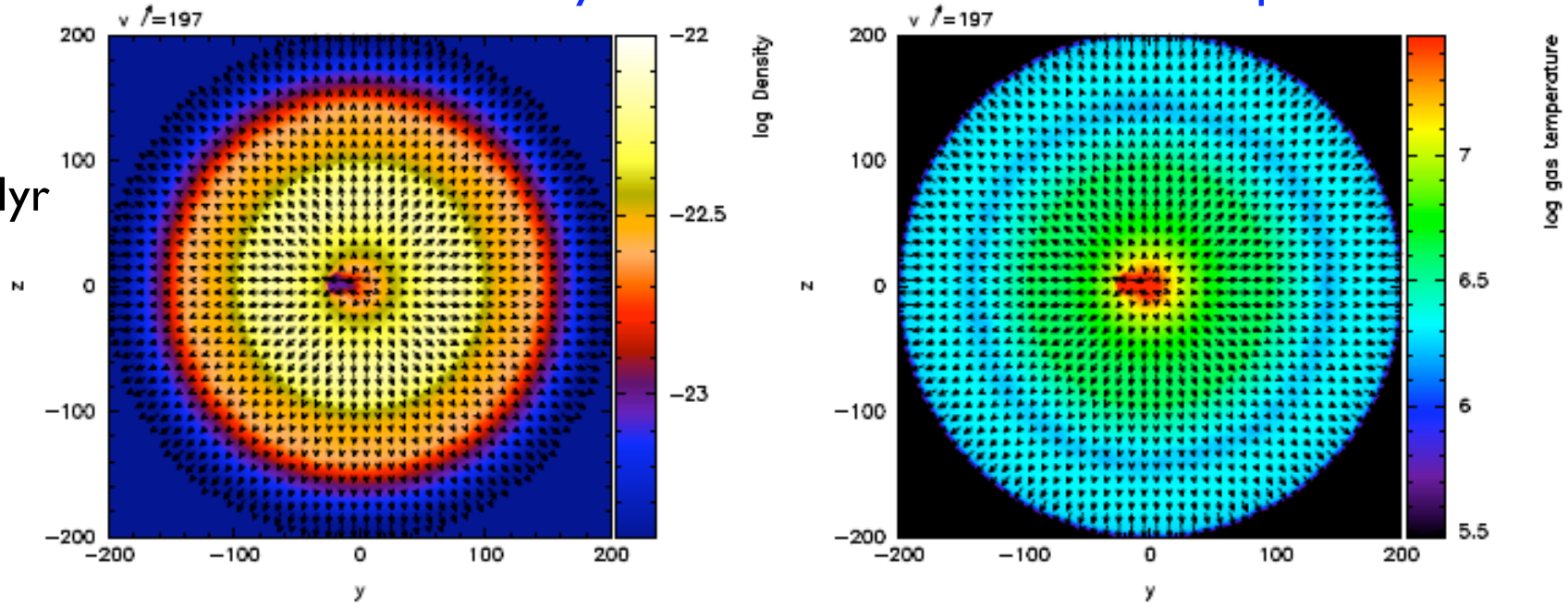

t = 3.0 Myr

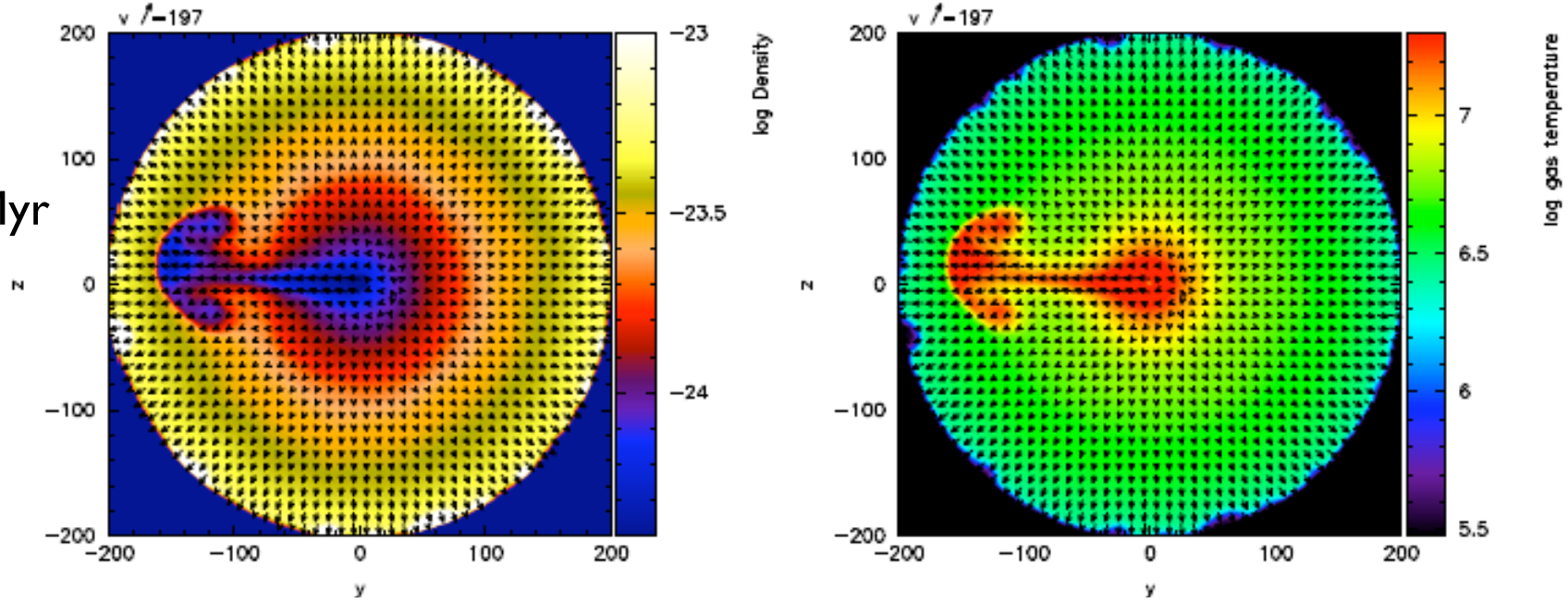

2

Introduction to Thermal Instability

- Gas can undergo catastrophic heating or cooling creating fragmentation & clumps
- Field 1965, ApJ, 142, 531
- Balbus 1995, ASPC, 80, 328

$$\left(\frac{\partial P}{\partial T}\right)_{\ell} < 0$$

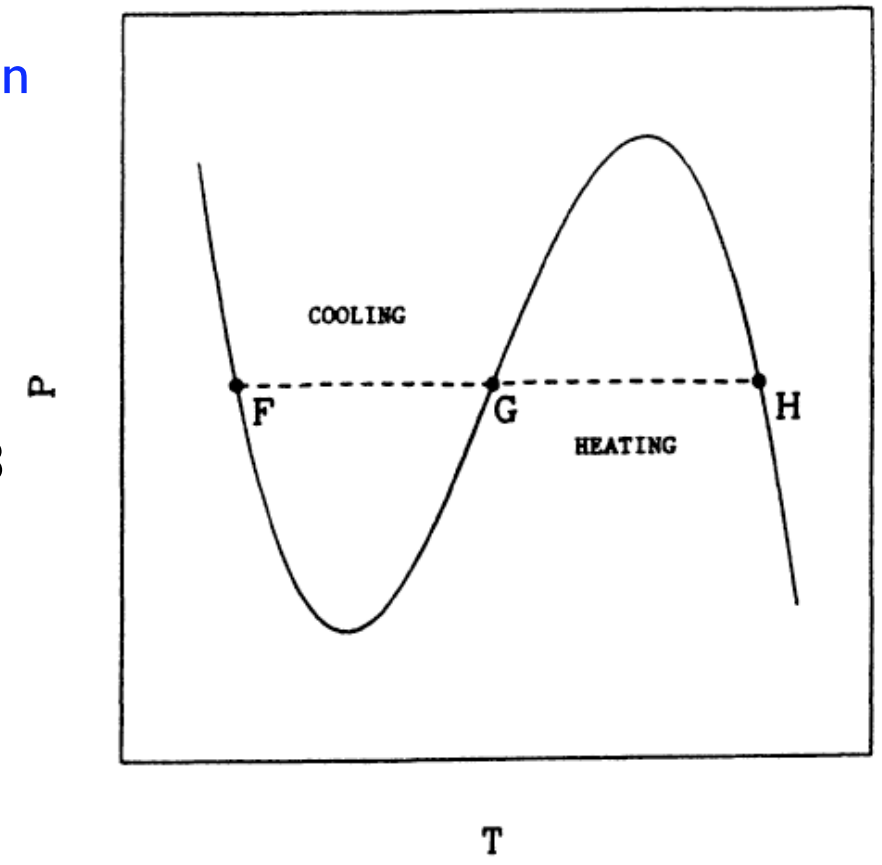

Figure 1. Schematic representation of multiple-phase cooling curve in the $P - T$ plane.

Pressure-ionization parameter :

$$\Xi = \frac{F_X}{cP_{\rm gas}}$$

Thermal Instability

$$\frac{dT}{d\Xi} < 0$$

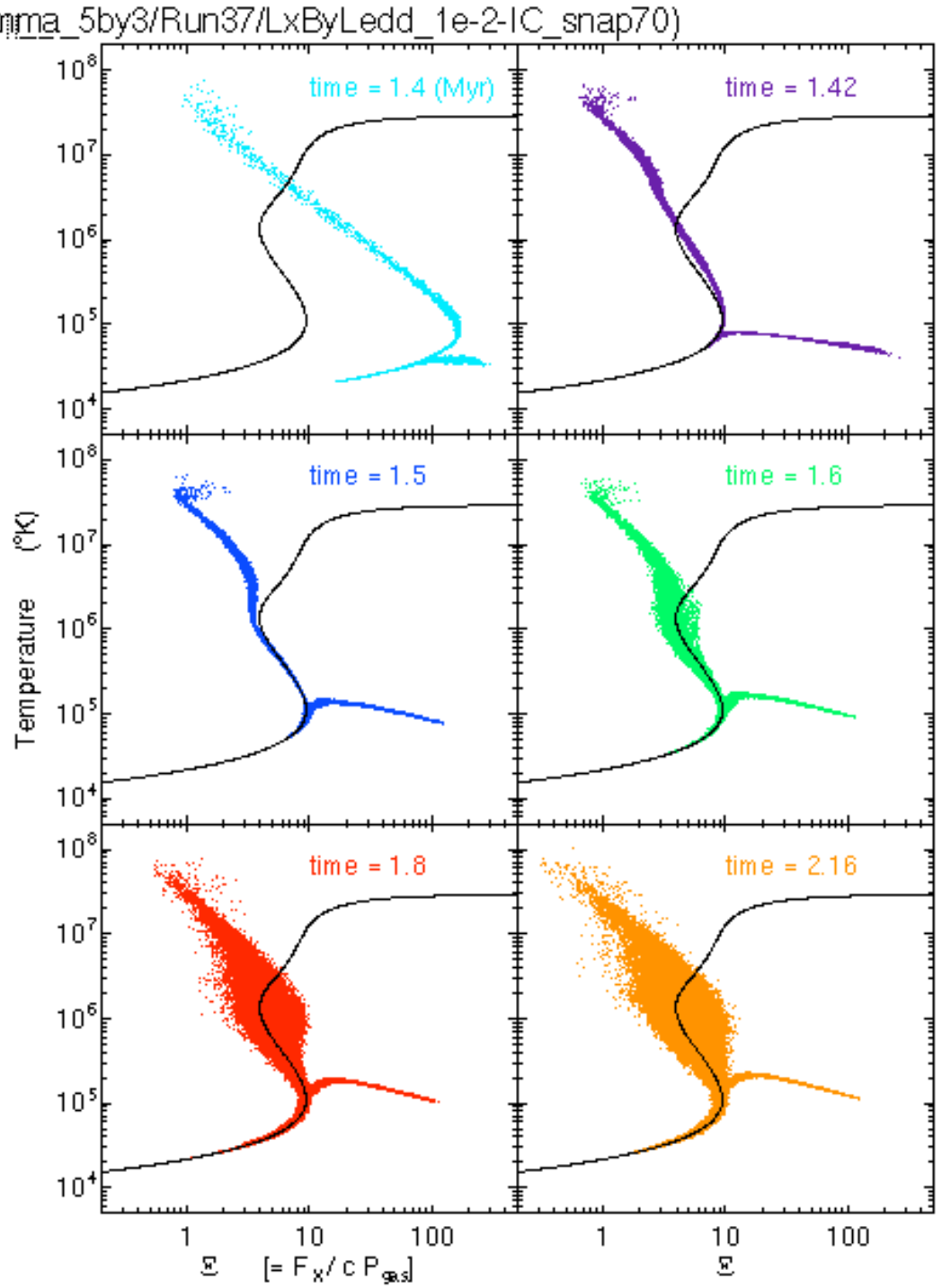

Analysing Thermal Instability

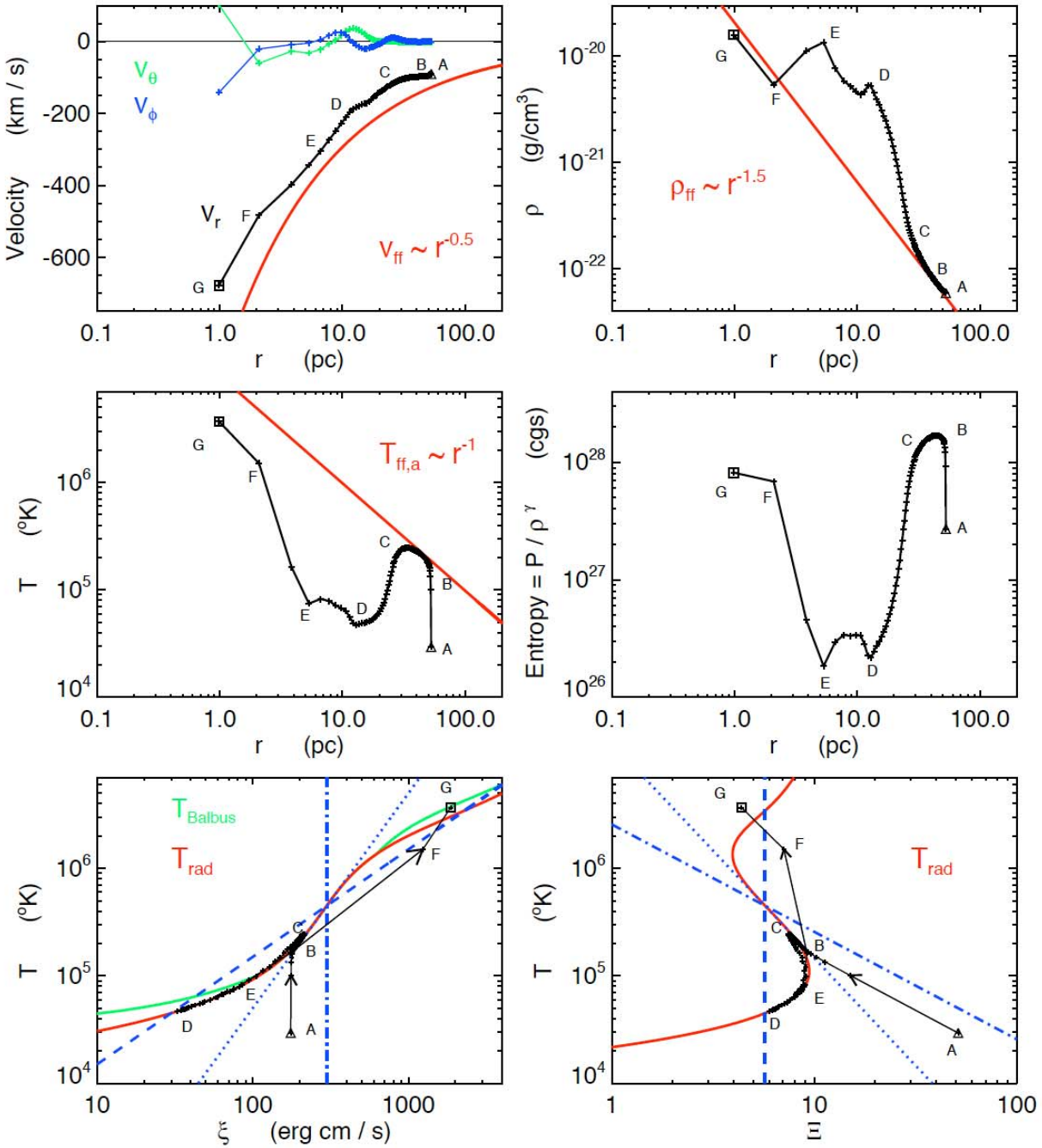

22-mars-13

Figure 4. Time evolution of a single particle in Run 26 as it moves inward. Letters A, B, C, D, E, F, G denote the major transition points on the track. The starting point (A) is denoted by the triangle in each panel, showing the initial condition at $t = 1.4$ Myr and $r = 53$ pc, The ending point (G) at $t = 1.8$ Myr and $r = 0.99$ pc is represented by the square in each panel. The plus signs denote the relevant

TI Timescales

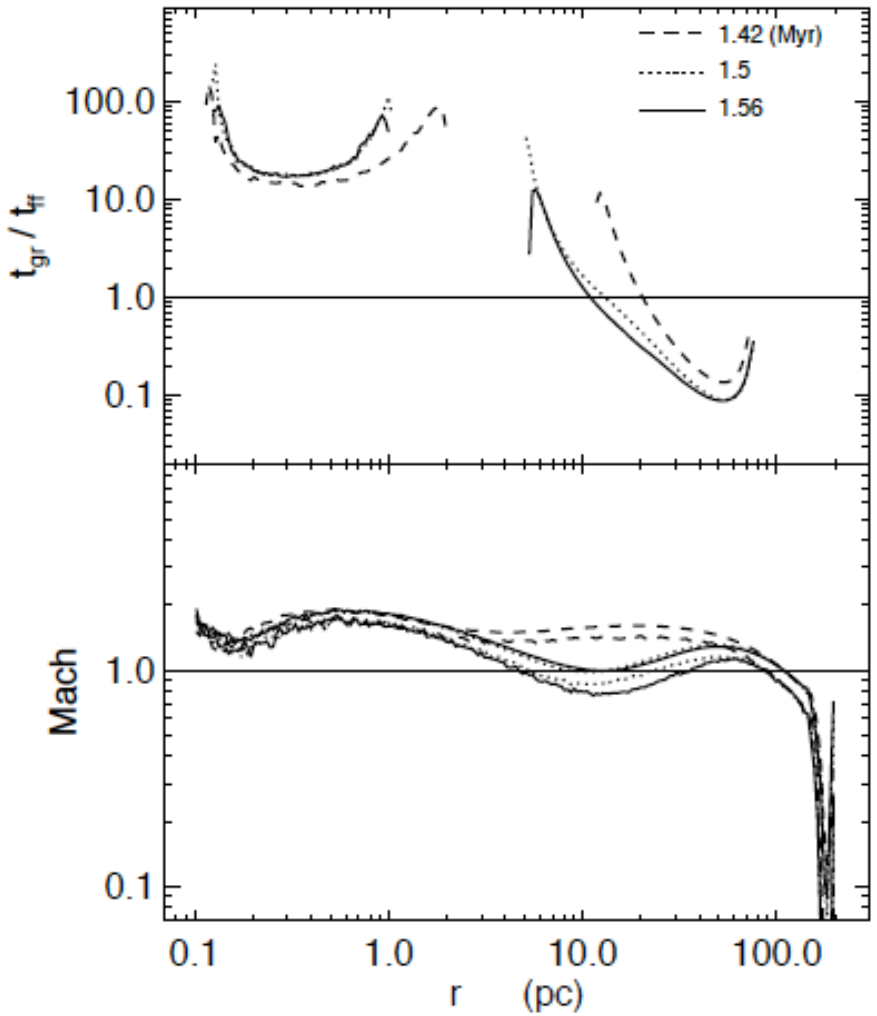

TI grows when:

- $t_{TI,gr} < t_{ff}$
- Subsonic flow

(Krolik & London 1983)

Figure 5. Ratio of thermal instability growth time (t_{gr}) and free-fall time (t_{ff}) in the top panel at three simulation epochs: $t = 1.42$ Myr (dashed curve), 1.5 Myr (dotted), and 1.56 Myr (solid), when the flow is still spherical. The ratio is plotted only at the radial ranges with a positive growth rate and represent regions where TI can grow. The radial gaps indicate regions which have negative growth rate and are stable to TI. Mach number in the bottom panel; the upper and lower curve of each linestyle denote the median and minimum Mach at a given radius. Details are described in §3.1.2.

Convective Instability (Brunt-Vaisala) Timescales

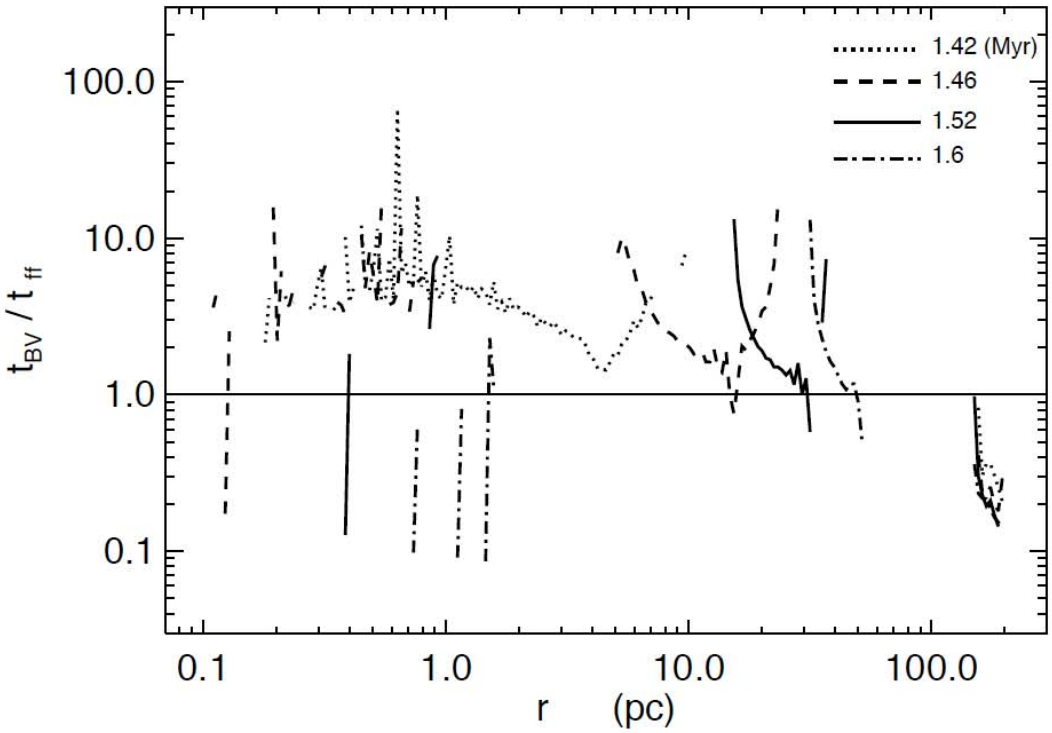

Flow becomes convectively unstable when:

- $t_{BV} < t_{ff}$

(Balbus & Soker 1989)

Figure 11. Ratio of the Brunt-Vaisala timescale (t_{BV}) for convective instability and free-fall time (t_{ff}) at four simulation epochs when the flow is nearly steady: $t = 1.42$ Myr (dotted), 1.46 Myr (dashed), 1.52 Myr (solid), and 1.6 Myr (dot-dash). The ratio is plotted only at the radial ranges having a real effective Brunt-Vaisala frequency ($\omega^2_{BV} > 0$) and represent convectively unstable regions. The radial gaps indicate regions which have imaginary frequency ($\omega^2_{BV} < 0$) and are convectively stable. The details are described in § 3.3.1.

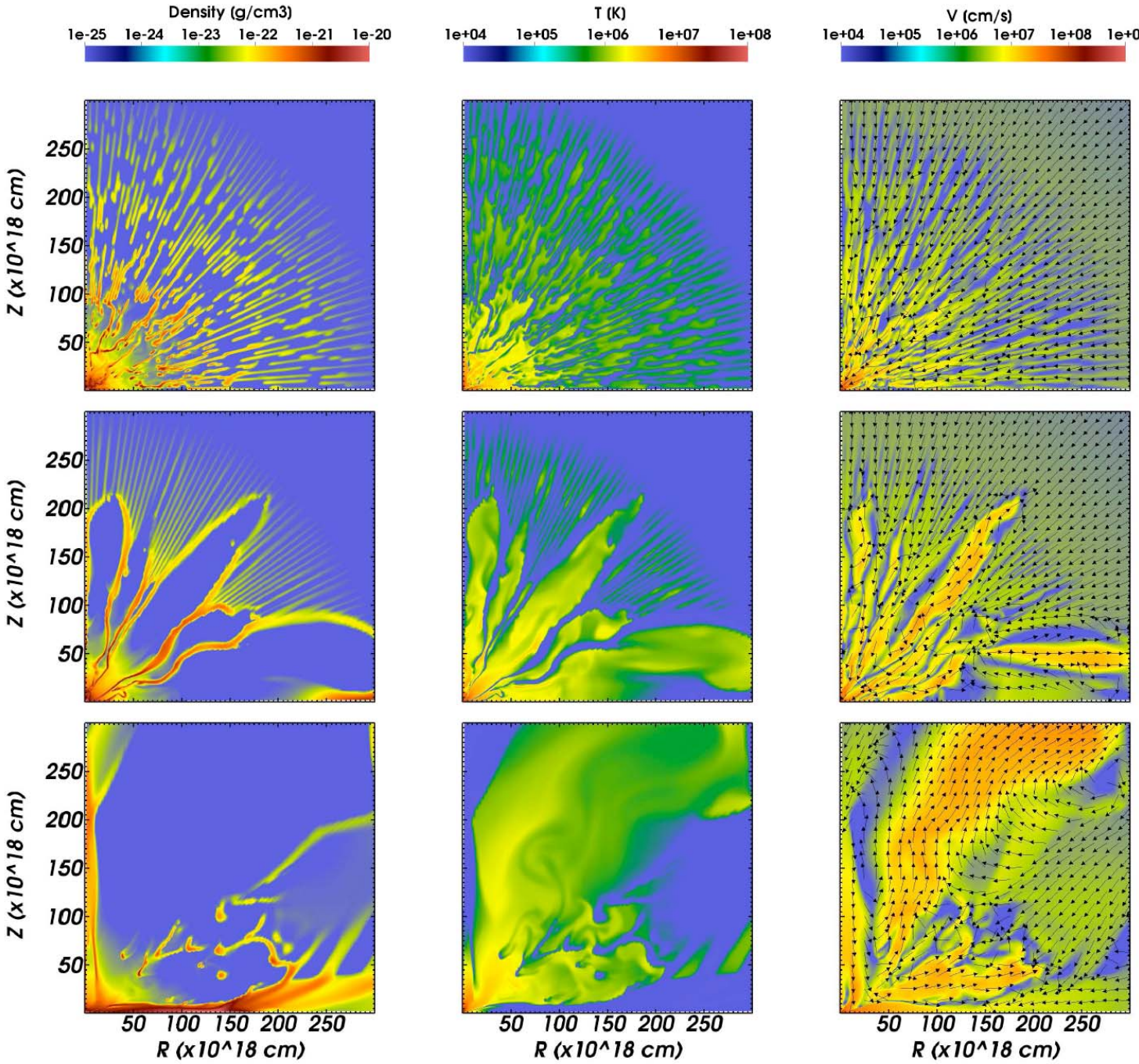

Consistent Results with ZEUS Code

(Moscibrodzka & Proga 2013, accepted in ApJ, arXiv:1303.2341)

FIG. 7.— Density, temperature, velocity magnitude with velocity direction (left, middle, and right column, respectively) in model 2D512x128D at t=3, 6 and 12 Myr (upper, middle, and bottom rows, respectively). Each panel show inner parts of the flow at $r \leq 100$ pc.

Conclusions

- SPH can reproduce Bondi accretion for several*t_{Bondi}, duration increasing with r_{out}
- Radiative heating & cooling has been incorporated in the code

- Current implementation of Artificial Viscosity in GADGET-III overheats gas near r_{in}

- Feedback by radiative heating
  - $\Rightarrow$ Increasing L_X reduces mass inflow rate, produces outflow

- Instability-driven fragmentation: cold clumps & hot bubbles
  - Thermal instability, and Convective instability
  - Formation of clouds in broad-line region and narrow-line region of AGN, star-formation, variability of AGN luminosity

- Future work
  - Include more physics: rotation, disk accretion, radiation pressure, …
  - Compare with BLR and NLR observations
  - Apply to cosmological simulations

Extra Slides

How does mass accretion rate (BH microphysics) depend on galaxy-scale gas properties?

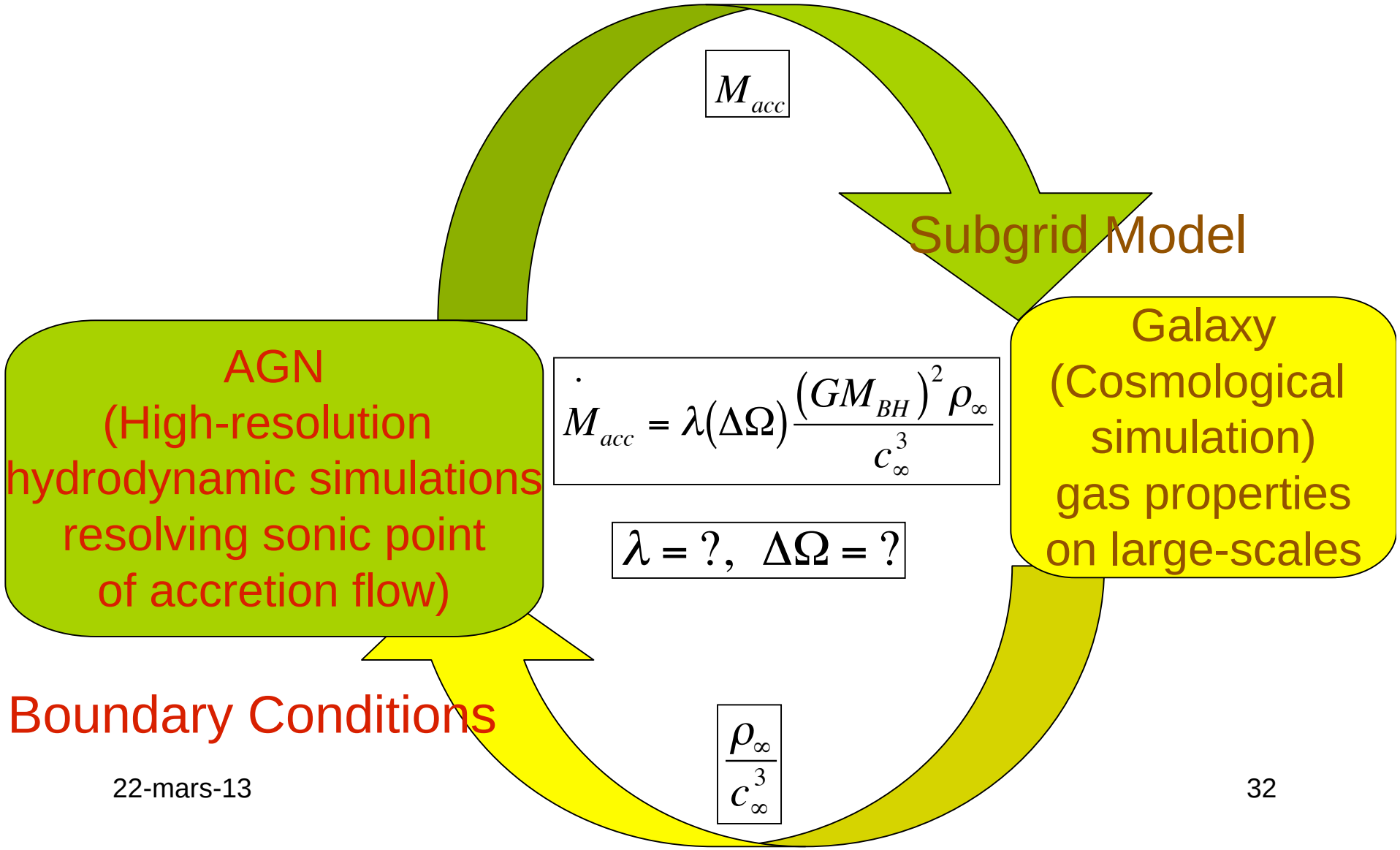

Artificial Viscosity in Gadget

shocks and no external sources of heat, the equations above already fully define reversible fluid dynamics in SPH. The entropy A_i of each particle remains constant in such a flow.

However, flows of ideal gases can easily develop discontinuities, where entropy is generated by microphysics. Such shocks need to be captured by an artificial viscosity in SPH. To this end, GADGET-2 uses a viscous force

$$\left.\frac{\mathrm{d}\boldsymbol{v}_i}{\mathrm{d}t}\right|_{\mathrm{visc}} = -\sum_{j=1}^{N} m_j \Pi_{ij} \nabla_i \overline{W}_{ij}, \tag{9}$$

where $\Pi_{ij} \geqslant 0$ is non-zero only when particles approach each other in physical space. The viscosity generates entropy at a rate

$$\frac{\mathrm{d}A_i}{\mathrm{d}t} = \frac{1}{2}\frac{\gamma-1}{\rho_i^{\gamma-1}} \sum_{j=1}^{N} m_j \Pi_{ij} \boldsymbol{v}_{ij} \cdot \nabla_i \overline{W}_{ij}, \tag{10}$$

transforming kinetic energy of gas motion irreversibly into heat. The symbol $\overline{W}_{ij}$ is here the arithmetic average of the two kernels $W_{ij}(h_i)$ and $W_{ij}(h_j)$.

The Monaghan–Balsara form of the artificial viscosity (Monaghan & Gingold 1983; Balsara 1995) is probably the most widely employed parametrization of the viscosity in SPH codes. It takes the form

$$\Pi_{ij} = \begin{cases} \left(-\alpha c_{ij}\mu_{ij} + \beta\mu_{ij}^2\right)/\rho_{ij} & \text{if } \boldsymbol{v}_{ij}\cdot\boldsymbol{r}_{ij} < 0 \\ 0 & \text{otherwise,} \end{cases} \tag{11}$$

with

$$\mu_{ij} = \frac{h_{ij}\,\boldsymbol{v}_{ij}\cdot\boldsymbol{r}_{ij}}{\left|\boldsymbol{r}_{ij}\right|^2}. \tag{12}$$

Here, h_{ij} and ρ_{ij} denote arithmetic means of the corresponding quantities for the two particles i and j, with c_{ij} giving the mean sound speed. The strength of the viscosity is regulated by the parameters α and β, with typical values in the range $\alpha \simeq 0.5$–1.0 and the frequent choice of $\beta = 2\,\alpha$.

In the equation of motion, the viscosity acts like an excess pressure $P_{\mathrm{visc}} \simeq (1/2)\rho_{ij}^2\Pi_{ij}$ assigned to the particles. For the new form (14) of the viscosity, this is given by

$$P_{\mathrm{visc}} \simeq \frac{\alpha}{2}\gamma\left[\frac{w_{ij}}{c_{ij}} + \frac{3}{2}\left(\frac{w_{ij}}{c_{ij}}\right)^2\right] P_{\mathrm{therm}}, \tag{15}$$

assuming roughly equal sound speeds and densities of the two particles for the moment. This viscous pressure depends only on a Mach-number-like quantity w/c, and not explicitly on the particle separation or smoothing length. We found that the modified viscosity (14) gives equivalent or improved results in our tests compared to the standard formulation of equation (11). In simulations with dissipation, this has the advantage that the occurrence of very large viscous accelerations is reduced, so that a more efficient and stable time integration results. For these reasons, we usually adopt the viscosity (14) in GADGET-2.

The signal-velocity approach naturally leads to a Courant-like hydrodynamical time-step of the form

$$\Delta t_i^{(\mathrm{hyd})} = \frac{C_{\mathrm{courant}}\,h_i}{\max_j(c_i + c_j - 3w_{ij})} \tag{16}$$

which is adopted by GADGET-2. The maximum is here determined with respect to all neighbours j of particle i.

Following Balsara (1995) and Steinmetz (1996), GADGET-2 also uses an additional viscosity-limiter to alleviate spurious angular momentum transport in the presence of shear flows. This is done by multiplying the viscous tensor with $(f_i + f_j)/2$, where

$$f_i = \frac{|\nabla\times\boldsymbol{v}|_i}{|\nabla\cdot\boldsymbol{v}|_i + |\nabla\times\boldsymbol{v}|_i} \tag{17}$$

is a simple measure for the relative amount of shear in the flow around particle i, based on standard SPH estimates for divergence and curl (Monaghan 1992).

The above equations for the hydrodynamics were all expressed using physical coordinates and velocities. In the actual simulation code, we use comoving coordinates $\boldsymbol{x}$, comoving momenta $\boldsymbol{p}$ and comoving densities as internal computational variables, which are

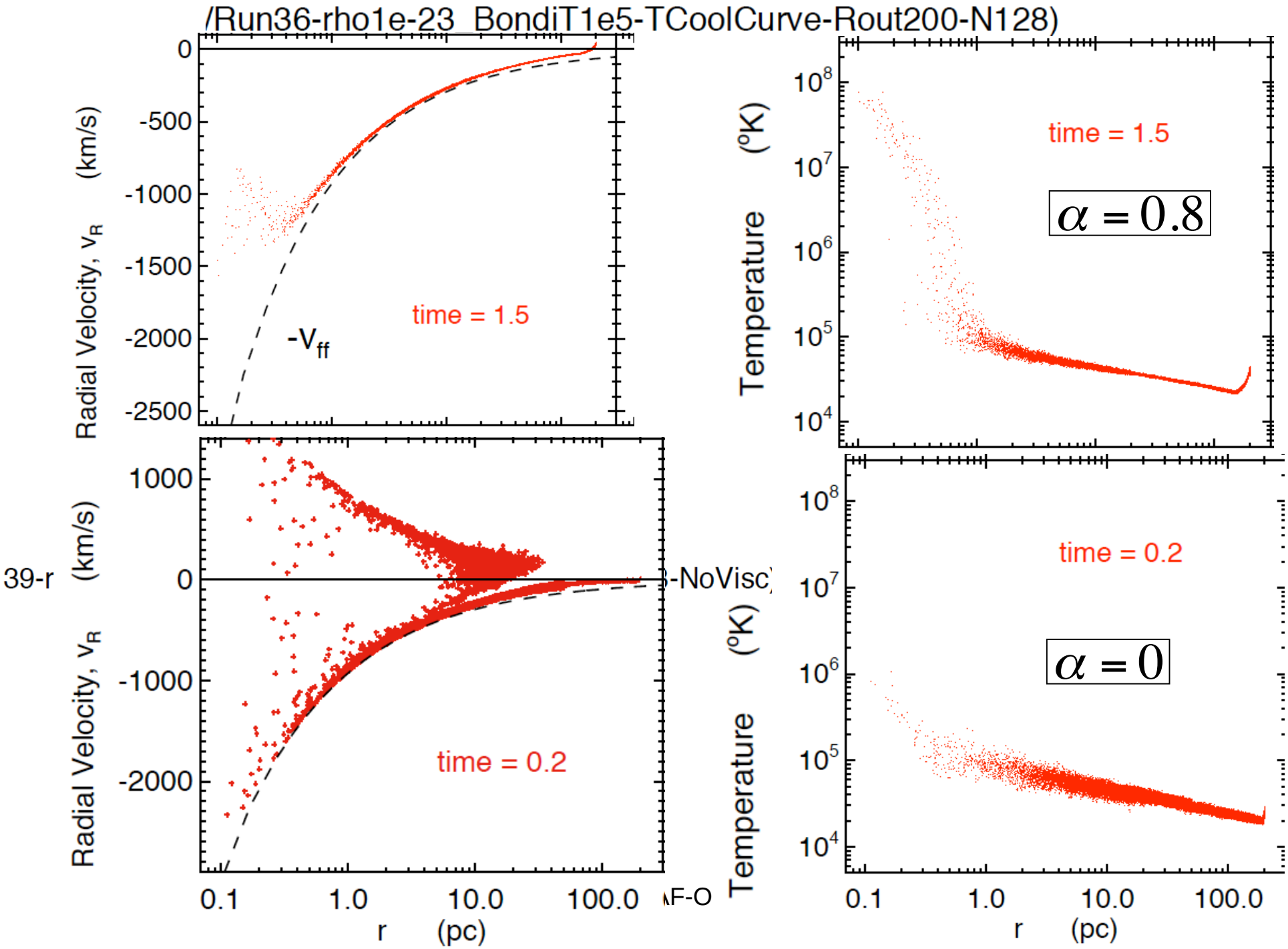
/Run36-rho1e-23_BondiT1e5-TCoolCurve-Rout200-N128)
Radial Velocity, v_R (km/s)
0
-500
-1000
-1500
-2000
-2500
$-V_{ff}$
time = 1.5
Temperature (^oK)
10^8
10^7
10^6
10^5
10^4
time = 1.5
$\alpha = 0.8$
39-r
-NoVisc)
Radial Velocity, v_R (km/s)
1000
0
-1000
-2000
time = 0.2
Temperature (^oK)
time = 0.2
$\alpha = 0$
0.1
1.0
10.0
100.0
r (pc)
0.1
1.0
10.0
100.0
r (pc)

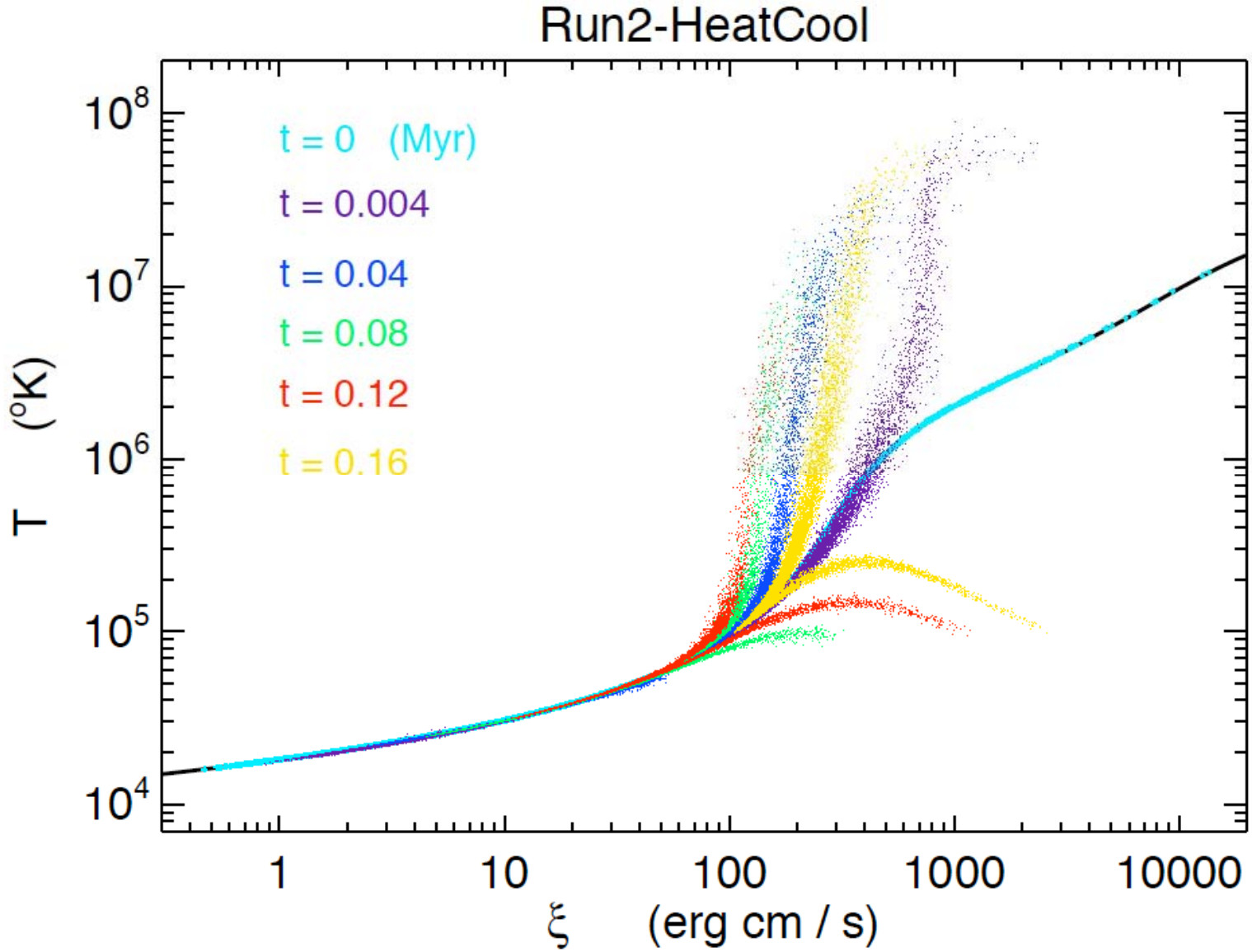

Temperature vs. photo-ionization parameter of particles overplotted with the implemented cooling curve.

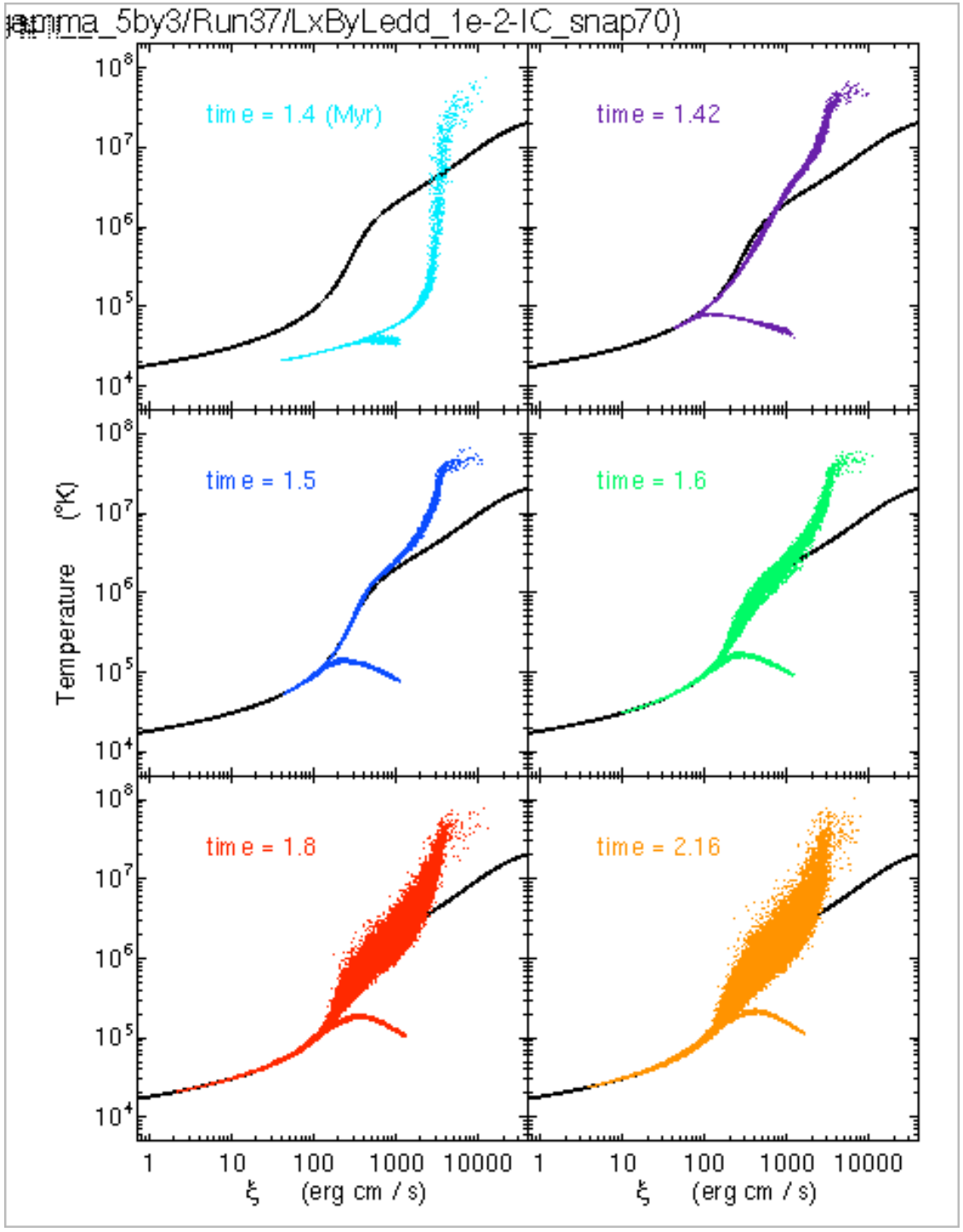
gamma_5by3/Run37/LxByLedd_1e-2-IC_snap70)
time = 1.4 (Myr)
time = 1.42
time = 1.5
time = 1.6
time = 1.8
time = 2.16
Temperature (°K)
ξ (erg cm / s)
ξ (erg cm / s)

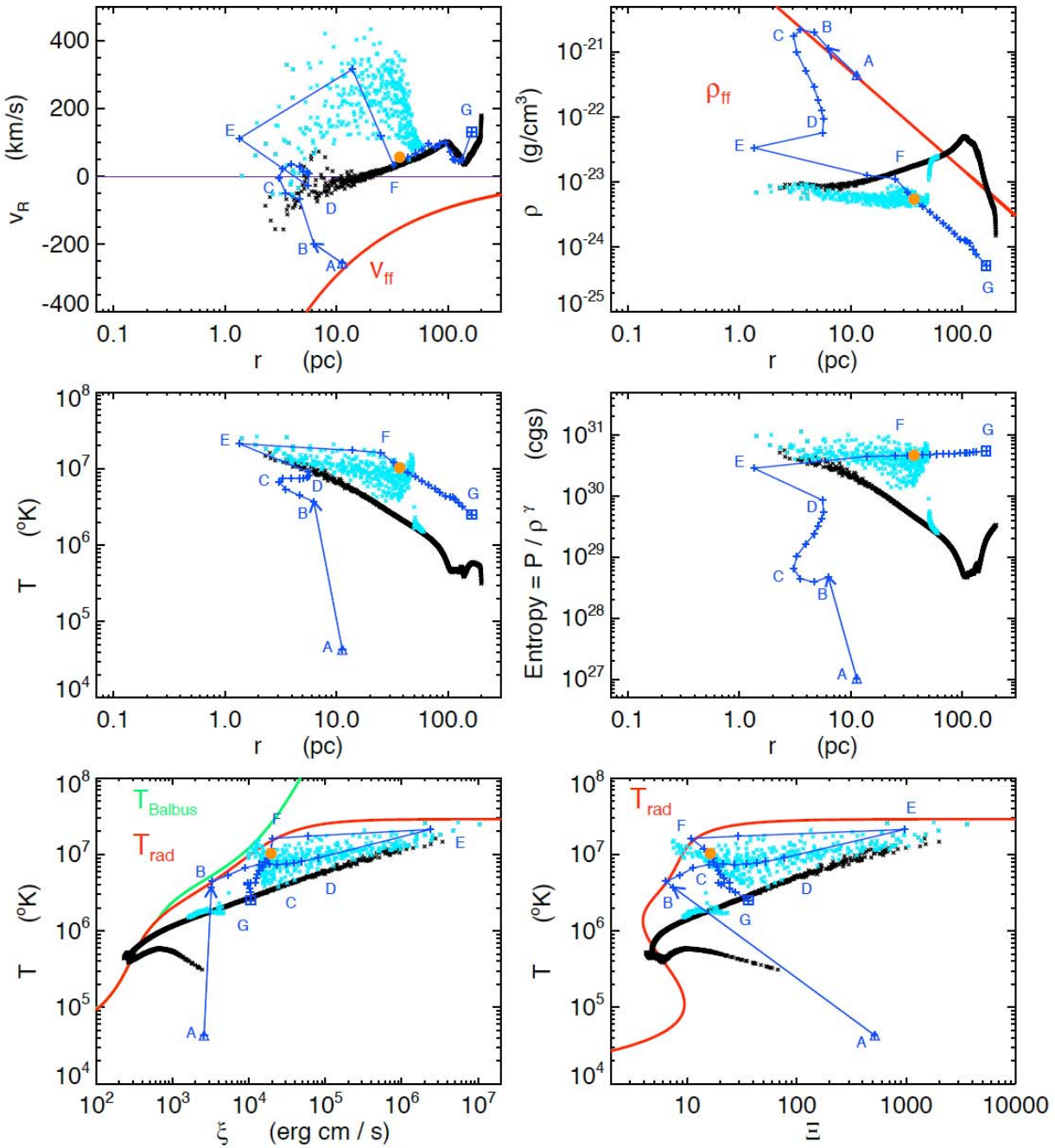

Figure 10. Properties of gas in Run 28 at $t = 2.0$ Myr shown as the cyan and black plus symbols. The cyan points are particles overlapping with the negative-y axis (through their smoothing lengths) at $r < 60$ pc hence belonging to the bubble, and the black points